

1

2

3

4

Iron isotope insights into equatorial Pacific biogeochemistry

5

6 Authors: Capucine Camin ¹, Marie Labatut¹, Catherine Pradoux¹, James W. Murray², François
7 Lacan¹

8

9 ¹ Université de Toulouse, LEGOS (CNES/CNRS/IRD/UT), Toulouse, France

10 ² School of Oceanography, University of Washington, Seattle, Washington, USA

11

12 Corresponding authors: Capucine Camin and François Lacan, LEGOS, 14 Avenue Edouard
13 Belin, F-31400 Toulouse, France (capucine.camin@orange.fr and francois.lacan@cnrs.fr).

14

15

ABSTRACT

The EUCFe cruise (RV *Kilo Moana*, 2006) was designed to characterize sources of Fe to the western equatorial Pacific and its transport by the Equatorial Undercurrent (EUC), a narrow and fast eastward current flowing along the equator, to the eastern equatorial Pacific High Nutrient Low Chlorophyll (HNLC) region. This study presents seawater dissolved (DFe) and particulate (PFe) iron concentrations and isotopic compositions ($\delta^{56}\text{DFe}$ and $\delta^{56}\text{PFe}$) from 15 stations in the equatorial band (2°N-2°S) between Papua New Guinea and 140°W, ~~that extends~~ ~~over~~ more than 8 500 km along the equator and in the upper 1 000 m of the water column.

$\delta^{56}\text{DFe}$ and $\delta^{56}\text{PFe}$ ranged from -0.22 to $+0.79 \pm 0.07$ ‰ and from -0.52 to $+0.43 \pm 0.07$ ‰, respectively (relative to IRMM-14, 95 % confidence interval). Source signatures, biogeochemical processes and transport all contribute to these observations. Two distinct areas, one under continental influence (the western equatorial Pacific) and an open ocean region (the central equatorial Pacific), emerged from the data. In the area under continental influence, high PFe concentrations along with $\delta^{56}\text{DFe}$ values systematically heavier than that of $\delta^{56}\text{PFe}$ indicated ~~an equilibrium fractionation and the co-occurrence of chemical fluxes from both phases toward the other. a permanent and reversible dissolved-particulate exchange.~~ This exchange occurs through non-reductive processes, as previously proposed from three of the eight stations of this area (Labatut et al., 2014) ~~and extends up to 1 200 km from the coast.~~ In the open ocean area, preservation of a DFe isotopic signature of $\sim +0.36$ ‰ within the EUC, from Papua New Guinea to the central equatorial Pacific (7 800 km), confirmed the origin of the DFe carried within this current toward the HNLC region. At the same depth, bordering the EUC at 2°N and 2°S at 140°W, light isotopic signatures suggested that ~~iron was iron~~ originating from the eastern Pacific oxygen minimum zones. These light signatures were also observed in deeper central waters, between 200 and 500 m. Our data did not allow conclusions about fractionation during uptake by phytoplankton, but indicated that ~~any this~~ ~~fractionation,~~ ~~must be if any, is small,~~ ~~if present, must be small,~~ no larger than a few tenths of a per mil.

KEY WORDS

Iron isotopes, equatorial Pacific Ocean, oxygen minimum zones, non-reductive dissolution, iron cycle, water masses.

1. INTRODUCTION

Iron (Fe) is an essential nutrient for phytoplankton, enabling them to fulfil their role as primary producers (Morel et al., 2020). Through its influence on primary productivity and plankton speciation, Fe plays a critical role in regulating the biological carbon pump and, consequently, the global carbon cycle and climate. Fe concentrations in the surface open ocean are often low (of the order of 0.1 nmol.kg^{-1}), potentially limiting primary productivity (Martin, 1992). Regions where Fe is limiting, despite the availability of macronutrients, are termed High Nutrient Low Chlorophyll (HNLC) areas. One notable HNLC region is the eastern equatorial Pacific (Chisholm and Morel, 1991), where Fe is believed to ~~be~~ have a main source from the western Pacific and transported eastward within the Equatorial Undercurrent (EUC) (Murray et al., 1994; Coale et al., 1996; Mackey et al., 2002; Kaupp et al., 2011). The EUC is an eastward-flowing subsurface current associated with upwellings that transports Fe from Papua New Guinea (PNG) toward South America along the equator (Gordon et al., 1997; Kaupp et al., 2011; Radic et al., 2011; Slemons et al., 2012; Winckler et al., 2016). Iron within the EUC is assumed to have both lithogenic and hydrothermal origins (Gordon et al., 1997). Specifically, the lithogenic component is suggested to primarily originate from rivers and sediments on the

62 PNG continental margin (Mackey et al., 2002; Slemons et al., 2010; Radic et al., 2011; Labatut
63 et al., 2014).

64 Although Fe concentration data are fundamental, isotopic measurements provide deeper
65 insight into both the provenance of Fe and internal processes governing its cycling (Lacan et
66 al., 2008; John et al., 2012; Conway and John, 2014; Ellwood et al., 2015). The isotopic
67 composition of Fe, expressed as $\delta^{56}\text{Fe}$ in per mil (‰), is defined as the deviation of the $^{56}\text{Fe}/^{54}\text{Fe}$
68 ratio of a sample from that of the IRMM-14 standard:

$$69 \quad \delta^{56}\text{Fe} = \frac{(^{56}\text{Fe}/^{54}\text{Fe})_{\text{sample}}}{(^{56}\text{Fe}/^{54}\text{Fe})_{\text{IRMM-14}}} - 1 \quad (\text{Equation 1})$$

70 The isotopic signatures can trace Fe from distinct sources, including fluvial inputs
71 (Fantle and DePaolo, 2004; Bergquist and Boyle, 2006; Ingri et al., 2006), sedimentary inputs
72 (Severmann et al., 2006; Homoky et al., 2009; Radic et al., 2011; Labatut et al., 2014),
73 hydrothermal inputs (Sharma et al., 2001; Severmann et al., 2004; Rouxel et al., 2008; Bennett
74 et al., 2009; [Resing et al., 2015](#)), and atmospheric inputs (Waeles et al., 2007; Flament et al.,
75 2008; Kurisu et al., 2016; Camin et al., 2025). They also provide information on internal oceanic
76 processes. Processes such as biological assimilation, dissolution, sorption, precipitation,
77 complexation and redox reactions, can modify the isotopic composition of Fe, through isotopic
78 fractionation.

79 Despite advances, substantial uncertainties remain regarding both the isotopic signature
80 of sources and the isotopic fractionation of processes. Hydrothermal and sedimentary sources
81 are poorly characterized due to limited understanding of the processes governing Fe exchange
82 and speciation. Additionally, the extent and mechanisms of isotopic fractionation remain
83 incompletely understood. For example, fractionation caused by phytoplankton during
84 biological uptake remains uncertain, with studies suggesting preferential uptake of either lighter
85 or heavier isotopes (Lacan et al., 2008; Radic et al., 2011; Conway and John, 2014; Ellwood et
86 al., 2015, 2020; Klar et al., 2018; [Sieber et al., 2021](#); [Tian et al., 2023](#); [John et al., 2024](#)).

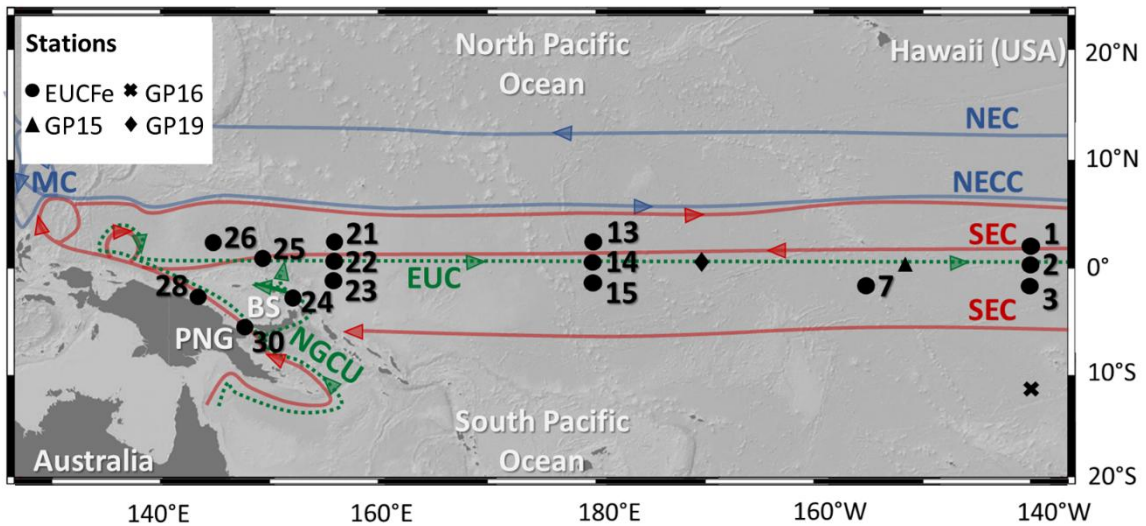
87 To better understand the sources, transport, and cycling of Fe in this region, the EUcFe
88 cruise (Equatorial Undercurrent Fe cruise) was conducted across the western and central
89 equatorial Pacific (RV Kilo Moana, PI: J. W. Murray, 2006). Iron isotope data from the EUcFe
90 cruise were previously published from four stations: three located in the west near PNG and
91 one in the open ocean (0° , 180°E) (Radic et al., 2011; Labatut et al., 2014). At the three stations
92 near PNG, an important source of dissolved Fe (DFe) was attributed to non-reductive exchange
93 processes between dissolved and mainly lithogenic particulate phases. The Fe isotope
94 signatures observed at the open ocean station indicated that in the deeper layer of the EUC the
95 Fe isotope signatures from the western Pacific were preserved toward the open ocean over more
96 than 4,000 km. The Fe isotopic composition of aerosols, collected during the cruise, was also
97 documented. Their slightly heavy signatures, $\delta^{56}\text{PFe} = +0.31 \pm 0.21 \text{‰}$ (2SD, $n = 9$), were
98 interpreted as reflecting isotopic fractionation due to partial dissolution of crustal dust during
99 atmospheric transport (Camin et al., 2025).

100 This present study reports Fe isotopic data from an additional 11 stations from the
101 EUcFe cruise in the equatorial band (2°N - 2°S) between Papua New Guinea and 140°W , over
102 more than 8,500 km along the equator and in the top 1 000 m of the water column. By expanding
103 the spatial coverage of concentration and isotopic measurements, we constrain the basin scale
104 Fe biogeochemical cycle in the western and central equatorial Pacific.

105

2. HYDRODYNAMICAL CONTEXT, WATER MASSES AND CURRENTS

107 Seawater samples (n=76) were collected during the EUCFe cruise from the surface to
 108 1 000 m depth in the western and central equatorial Pacific Ocean. This area is influenced by
 109 the South and the North Pacific subtropical gyres that shape the large-scale circulation. The
 110 equatorial branches of those gyres are westward currents [extending from the surface to](#)
 111 [approximately 400 m depth](#) (Cravatte et al., 2017): the North Equatorial Current (NEC) and the
 112 South Equatorial Current (SEC). The main surface and subsurface currents and the EUCFe
 113 stations with $\delta^{56}\text{Fe}$ data are represented in Figure 1.



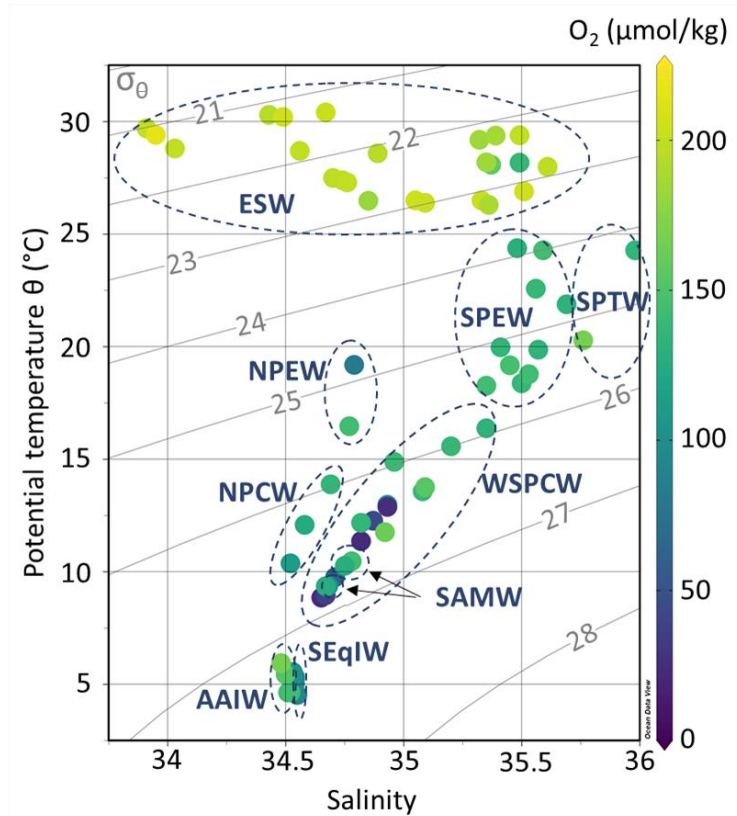
114

115 Figure 1. Map of the EUCFe stations and some [GP15](#), GP16 and GP19 stations. Main surface
 116 and subsurface currents are represented, in blue those carrying water masses of northern origins,
 117 in red those carrying waters of southern origins and in dashed green the undercurrents. BS:
 118 Bismarck Sea; EUC: Equatorial UnderCurrent; MC: Mindanao Current; NEC: North Equatorial
 119 Current; NECC: North Equatorial CounterCurrent; NGCU: New Guinea Coastal Undercurrent;
 120 SEC: South Equatorial Current (Delcroix et al, 1992; Fine et al, 1994; Kashino et al, 1996,
 121 2007; Johnson et al, 2002; Tomczak and Godfrey, 2003).

122 One of the specific structures of this circulation is the Equatorial Undercurrent (EUC).
 123 It is an intense subsurface equatorial current, with velocities up to $1 \text{ m}\cdot\text{s}^{-1}$ (Philander, 1973),
 124 flowing along the equator over 14,000 km (Tomczak and Godfrey, 2003). Its core rises toward
 125 the surface eastward, ~~from at~~ an average depth of 200 m in the western equatorial Pacific, ~~to at~~
 126 ~~a depths~~ of 130 m in the central equatorial Pacific and ~~at a depth of~~ 40 m in the eastern equatorial
 127 Pacific (Tomczak and Godfrey, 2003; Talley et al., 2011). It is fed by waters from the Low-
 128 Latitude Western Boundary Currents (LLWBCs) composed at two-thirds by southern currents
 129 (New Guinea Coastal Current, New Guinea Coastal Undercurrent, New Ireland Coastal
 130 Undercurrent) and at one-third by northern currents (Mindanao Current) (Tsuchiya et al., 1989;
 131 Butt and Lindstrom, 1994; Fine et al., 1994; Rodgers et al., 2003; Grenier et al., 2011). The
 132 EUC is therefore enriched with nutrients of continental origins and plays an essential role
 133 supplying the eastern equatorial Pacific HNLC area through the equatorial upwelling (Coale et
 134 al., 1996; Ryan et al., 2006; Slemons et al., 2009; Kaupp et al., 2011).

135 Below the EUC, there is a westward subsurface flow, the Equatorial Intermediate Current
 136 (EIC). The EIC is bounded by eastward North and South Subsurface Countercurrents (NSCC
 137 and SSSC) centered around 2°N and 2°S , not shown in Figure 1 (Tomczak and Godfrey, 2003;
 138 Cravatte et al., 2017).

139



140

141 Figure 2. Potential temperature (θ , °C), salinity (S), dissolved oxygen concentrations (O_2 ,
 142 $\mu\text{mol.kg}^{-1}$) of EUCFe samples. Isopycnals are shown in gray lines (σ_θ , kg.m^{-3}). The dashed
 143 ellipses show water masses: Equatorial Surface Water (ESW), South Pacific Tropical Water
 144 (SPTW), South Pacific Equatorial Water (SPEW), North Pacific Equatorial Water (NPEW),
 145 Western South Pacific Central Water (WSPCW), North Pacific Central Water (NPCW), South
 146 Antarctic Mode Water (SAMW), South Equatorial Intermediate Water (SeqIW) and Antarctic
 147 Intermediate Water (AAIW).

148 Table 1. Water masses identified during the EUCFe cruise, with their characteristics in the study
 149 area: origin, depth, potential temperature (θ , °C), salinity, potential density anomaly (σ_θ , kg.m^{-3})
 150 and dissolved oxygen concentration (O_2 , $\mu\text{mol.kg}^{-1}$). ~~Where t~~The currents ~~where they~~ flow is
 151 ~~are~~ specified. Currents acronym meanings are available in Figure 1, except for the North
 152 Equatorial Subsurface Current (NESC), the South Equatorial Subsurface Current (SESC) and
 153 the New Ireland Coastal Undercurrent (NICU).

154

Water Masses	Origin	EUCFe zone	Depth (m)	θ (°C)	Salinity	σ_{θ} (kg. m ⁻³)	O ₂ (μ mol. kg ⁻¹)	Currents	Characteristics	References
Equatorial Surface Water (ESW)	Mixing between the Tropical Surface Water and the Subtropical Surface Water, equatorial upwellings, advection of the Peru Current Water	Entire zone	0 - 100	21.0 - 30.5	33.5 - 35.7	20.5 - 23.5	108 - 193	SEC, NGCC, NICU, EUC	/	Fiedler & Talley, 2006; EUCFe sensor data
South Pacific Tropical Water (SPTW)	Subduction of surface waters in the tropics in a high-salinity area (evaporation excess) around the Polynesian region	Southeastern stations (stations 3 and 15)	100 - 200	18 - 25	35.7 - 36.7	24.3 - 25.3	134 - 167	SEC, NGCU, NGCC, NICU, EUC	Subsurface salinity maximum	Tsuchiya et al., 1989; Qu & Lindstrom, 2002; EUCFe sensor data
South Pacific Equatorial Water (SPEW)	Subduction of surface waters in the tropics in a high-salinity area (evaporation excess) around the Polynesian region: one branch, less salty, of the SPTW	Mainly western equatorial and southwestern stations	100 - 200	18 - 25	35.3 - 35.8	23.8 - 25.6	129 - 145	SEC, NICU, NGCU, NGCC, EUC	/	Tomczak & Hao, 1989; Tsuchiya et al., 1989; Qu & Lindstrom, 2002; Tomczak & Godfrey, 2003; EUCFe sensor data
North Pacific Equatorial Water (NPEW)	Mixture between SPEW and NPCW	Northern stations (stations 1 and 26)	100 - 200	16 - 20	34.7 - 35.0	24.3 - 25.5	80 - 145	NEC, EUC	Salinity minima of tropical waters	Tomczak & Godfrey, 2003; EUCFe sensor data
North Pacific Central Water (NPCW)	Northern subtropical front	Northwestern stations (stations 13, 21, 26)	200 - 300	10 - 17	33.5 - 34.7	25.2 - 26.4	110 - 135	EUC	Salinity minima of central waters	Emery & Meincke, 1986; Pickard & Emery, 1990; Tomczak & Godfrey, 2003; Grenier, 2012; EUCFe sensor data
Western South Pacific Central Water (WSPCW)	Subtropical convergence zone between Tasmania and New Zealand	Equatorial and southern stations and some northern stations	170 - 500	8.9 - 17	34.7 - 35.5	26.1 - 26.9	20 - 160	SEC, NGCU, NICU, EUC, EIC, NSCC, SSSC	Salinity maximum of central waters	Tsuchiya, 1981; Tomczak & Hao, 1989; Tsuchiya et al., 1989; Sokolov & Rintoul, 2000; Qu & Lindstrom, 2002; Tomczak & Godfrey, 2003; Qu et al., 2009; Grenier, 2012; EUCFe sensor data
South Antarctic Mode Water (SAMW)	Vertical convective overturning at the end of winter north of the Antarctic Circumpolar Current	Western stations (stations 22, 24, 25)	350 - 600	8.0 - 9.5	34.6 - 34.75	26.7 - 26.9	100 - 145	EIC, SEC	/	McCartney, 1977; Sokolov & Rintoul, 2000; EUCFe sensor data
South Equatorial Intermediate Water (SEqIW)	Mixing of AAIW and Pacific Deep Water	Every sample between 700 and 1000 m depth except the Southernmost stations close to the Bismarck Sea	700 - 1000	4.4 - 5.6	34.5 - 34.6	27.2 - 27.4	80 - 105	EIC, NSCC, SSSC, NESC, SESC	/	Wyrčki, 1962; Bingham & Lukas, 1995; Bostock et al., 2010; EUCFe sensor data
Antarctic Intermediate Water (AAIW)	Subduction of fresh surface water at the subantarctic front, west of the Drake Passage	Southernmost stations in the Bismarck Sea: at less than 60 km from Papua New Guinea coast (stations 24, 28, 30)	700 - 1000	4.7 - 6.0	34.4 - 34.6	27.2 - 27.3	140 - 170	SEC, NGCU, NGCC, NICU	Salinity minima of intermediate waters	Tsuchiya, 1991; Tsuchiya and Talley, 1996; Talley et al., 2011; EUCFe sensor data

156 In the equatorial Pacific Ocean between 140°E and 140°W, at least 9 different water
157 masses can be observed in the upper 1 000 m of the water column. Their θ , S and $[O_2]$
158 characteristics are shown in Figure 2 and reported in Table 1. The upper 100 m are mainly
159 composed of the Equatorial Surface Water (ESW), characterized by high temperatures and
160 oxygen concentrations. ESW is mainly formed from two water masses (Tropical Surface Water
161 (TSW) and Subtropical Surface Water (STSW)). Those are formed in the tropics where
162 evaporation exceeds precipitation and then transported toward the equator by the North and
163 South subtropical gyres. Due to mixing with upwelled waters, ESW is colder than TSW and
164 STSW (Fiedler and Talley, 2006). Between 100 and 200 m, there are three water masses, from
165 the saltiest to the freshest: the South Pacific Tropical Water (SPTW), the South Pacific
166 Equatorial Water (SPEW), the North Pacific Equatorial Water (NPEW) (Tsuchiya et al., 1989;
167 Lacan and Jeandel, 2001; Grenier et al., 2013). The SPTW originates from surface waters
168 subduction in the tropical South Pacific, a high-salinity area with excess evaporation (Tsuchiya
169 et al., 1989). The SPEW is a less salty version of the SPTW and the prevailing water mass
170 around the equator at these depths. It is the major constituent of the upper part of the EUC (σ_θ
171 $< 25.6 \text{ kg.m}^{-3}$) (Lacan and Jeandel, 2001; Tomczak and Godfrey, 2003; Grenier et al., 2011;
172 Grenier, 2012). The NPEW is formed by mixing of the SPEW and the North Pacific Central
173 Water (NPCW) (Tomczak and Godfrey, 2003). Between 200 and 500 m depth, central waters,
174 defined by a linear region on temperature-salinity diagrams, are found (Pollard et al., 1996;
175 Stramma and England, 1999; Tomczak and Godfrey, 2003). The Western South Pacific Central
176 Water (WSPCW), formed in the subtropical convergence zone between Tasmania and New
177 Zealand, is the major constituent of the lower part of the EUC ($\sigma_\theta > 25.6 \text{ kg.m}^{-3}$) (Tomczak and
178 Hao, 1989; Grenier et al., 2011; Grenier, 2012;). WSPCW is also the predominant water mass
179 at these depths in the study area. The North Pacific Central Water (NPCW) is formed in the
180 northern subtropical front (Tomczak and Godfrey, 2003). NPCW is found in the northern part
181 of the study area. Between 350 and 600 m, there is also the South Antarctic Mode Water
182 (SAMW), a water mass formed by vertical convective overturning at the end of the winter north
183 of the Antarctic Circumpolar Current (McCartney, 1977; Sokolov and Rintoul, 2000). The
184 SAMW is often associated with the Antarctic Intermediate Water (AAIW), a deeper water
185 mass. Both water masses, SAMW and AAIW, are found in the western part of the study area.
186 Between 600 and 1 000 m, two intermediate waters can be identified: the Equatorial
187 Intermediate Water (EqIW) and the AAIW. Some scientists refer to EqIW as part of the
188 Antarctic Intermediate Water (AAIW) (Yuan and Talley, 1992; Talley, 1999, 2008; Qu and
189 Lindstrom, 2004). In this article, the distinction between the EqIW and AAIW is relevant for
190 studying key parameters such as oxygen, nutrient concentrations and salinity along the equator.
191 The AAIW is formed by subduction of fresh surface water at the subantarctic front, west of the
192 Drake Passage (Tsuchiya, 1991; Talley et al., 2011). The EqIW is a mixing of AAIW and
193 Pacific Deep Water (formed without contact with the atmosphere by Antarctic Bottom Water,
194 Atlantic Deep Water and AAIW mixing) (Tomczak and Godfrey, 2003; Bostock et al., 2010).
195 It constitutes the predominant water mass at these depths in the study region.

196

197 3. SAMPLING AND ANALYTICAL PROCEDURES

198 Sampling and analytical procedures have been previously described (Radic et al., 2011;
199 Labatut et al., 2014). They are summarized below.

200 Seawater was sampled from surface to 1 000 m depth using acid cleaned Go-Flo bottles
201 (12 L) mounted on a trace metal rosette equipped with a CTD, lent by the University of Victoria
202 (Canada). Sample filtration was performed onboard in a homemade plastic room pressurized
203 with filtered air, with acid-cleaned Nuclepore™ membranes (0.4 μm pore size, 90 mm

204 diameter) housed in Teflon filter holders (Savillex™). After filtration, 10 liters of filtered
205 seawater were stored in acid-cleaned polyethylene containers and membranes were stored in
206 acid-cleaned Petri dishes.

207 Samples were processed and analyzed at the LEGOS laboratory (Observatoire Midi-
208 Pyrénées, Toulouse, France) between 2009 and 2012. All chemical procedures were conducted
209 in a trace-metal-clean laboratory under an ISO4 laminar flow hood, using high purity reagents
210 and acid cleaned labware.

211 Particles were fully digested in a mixture of 5 M HCl, 2.1 M HNO₃, and 0.6 M HF at
212 130 °C for 3 hours. To verify the completeness of the digestion, selected filters were re-digested,
213 confirming no particulate Fe (PFe) remained. ~~Leachate a~~ Aliquots (2 %) were reserved for Al
214 concentration measurements using an Element-XR HR-ICP-MS. A ⁵⁷Fe-⁵⁸Fe double spike was
215 added to the remaining 98 % of the ~~digested material leachates~~ and to filtered seawater, in
216 preparation for isotopic analyses. Dissolved iron was preconcentrated from filtered seawater on
217 a NTA Superflow resin, at pH = 1.8. Fe was purified from both types of samples with AG1-X4
218 anionic resin. Iron isotopic compositions and concentrations were measured with a Neptune
219 MC-ICP-MS.

220 Uncertainties are reported at a 95 % confidence level throughout this article. For Fe
221 concentrations and isotope measurements on the Neptune, the total procedural recovery was
222 93 ± 25 % for PFe and 86 ± 33 % for DFe. The total procedural blanks were 0.74 ± 1.17 ng
223 (2SD) for DFe and 7.47 ± 1.09 ng (2SD) for PFe. This amounts to 0.5 % and 0.6 % of the
224 samples average Fe content for DFe and PFe, respectively and 2.8% and 9.7 % for the sample
225 with the smallest Fe content for DFe and PFe, respectively. ~~was 0.6 % for PFe and 0.5 % for~~
226 ~~DFe of the average concentration and 9.6 % for PFe and 5.0 % for DFe of the least concentrated~~
227 ~~sample.~~ For DFe, the filtered seawater from a sample was divided into several aliquots, then
228 each was processed individually (including different double spiking, preconcentration and
229 purification). For PFe, each sample, i.e., membrane, was first digested (no division of the
230 membrane before digestion), then the digested sample was divided into several aliquots, and
231 each was processed individually (including different double spiking and purification). In some
232 instances, duplicate samples are taken at sea, from the same cast. These replicates are termed
233 "Go-Flo replicates" in the Table A1. Repeatability was 8 % for DFe concentrations, 4 % for
234 PFe concentrations, 0.05 ‰ for δ^{56} DFe and 0.04 ‰ for δ^{56} PFe. This level of precision is better
235 than the long-term external precision of 0.07 ‰, determined from repeated analyses of an in-
236 house "ETH Hematite" isotopic standard. As a result, uncertainties for δ^{56} Fe data are reported
237 as either ± 0.07 ‰ or the internal measurement uncertainty (2 standard errors), whichever is
238 larger.

239 The LEGOS Fe isotope protocol has been validated through intercalibration and
240 intercomparison exercises (Boyle et al., 2012; Conway et al., 2016) and detailed in Lacan et al.
241 (2008, 2010, 2021). Accuracy (~~referring to the two concepts of~~ trueness and precision) of
242 elemental concentrations measured by HR-ICP-MS was regularly verified using the certified
243 SLRS-5 river water material and through intercalibration exercises (Yeghicheyan et al., 2013,
244 2019).

245

246 4. RESULTS

247 Concentrations and isotopic compositions of DFe and PFe in seawater are reported in
248 Table 2. Previously published data from four stations (14, 24, 28 and 30) are included here for
249 clarity (Radic et al., 2011; Labatut et al., 2014). All Fe concentrations, Fe isotopic compositions,
250 temperature, salinity, oxygen data and an intercalibration report, have been ~~submitted to~~

251 included in the GEOTRACES Data Product. They are also available on the SEANOE open data
 252 repository (Lacan et al., 2025).

253 Table 2. Location, depth, hydrological properties, concentration and isotopic composition of
 254 dissolved and particulate Fe (DFe and PFe). Concentration relative uncertainties are 8.0 % for
 255 DFe and 4.3 % for PFe (95% confidence level). U95 stands for measurement uncertainty at the
 256 95 % confidence level. For most samples, dissolved O₂ concentration was measured in the
 257 samples onboard. When direct measurements were not available, as indicated by the (*) symbol,
 258 oxygen concentrations from the oxygen sensor on the rosette were used following calibration
 259 with in situ data. The (+) and (°) symbols indicate data previously published by Radic et al.
 260 (2011) and Labatut et al. (2014), respectively. ESW: Equatorial Surface Water; SPTW: South
 261 Pacific Tropical Water; SPEW: South Pacific Equatorial Water; NPEW: North Pacific
 262 Equatorial Water; NPCW: North Pacific Central Water; WSPCW: Western South Pacific
 263 Central Water; SAMW: South Antarctic Mode Water; SEqIW: South Equatorial Intermediate
 264 Water; AAIW: Antarctic Intermediate Water; Chloro. Max: Chlorophyll Maximum layer.

265

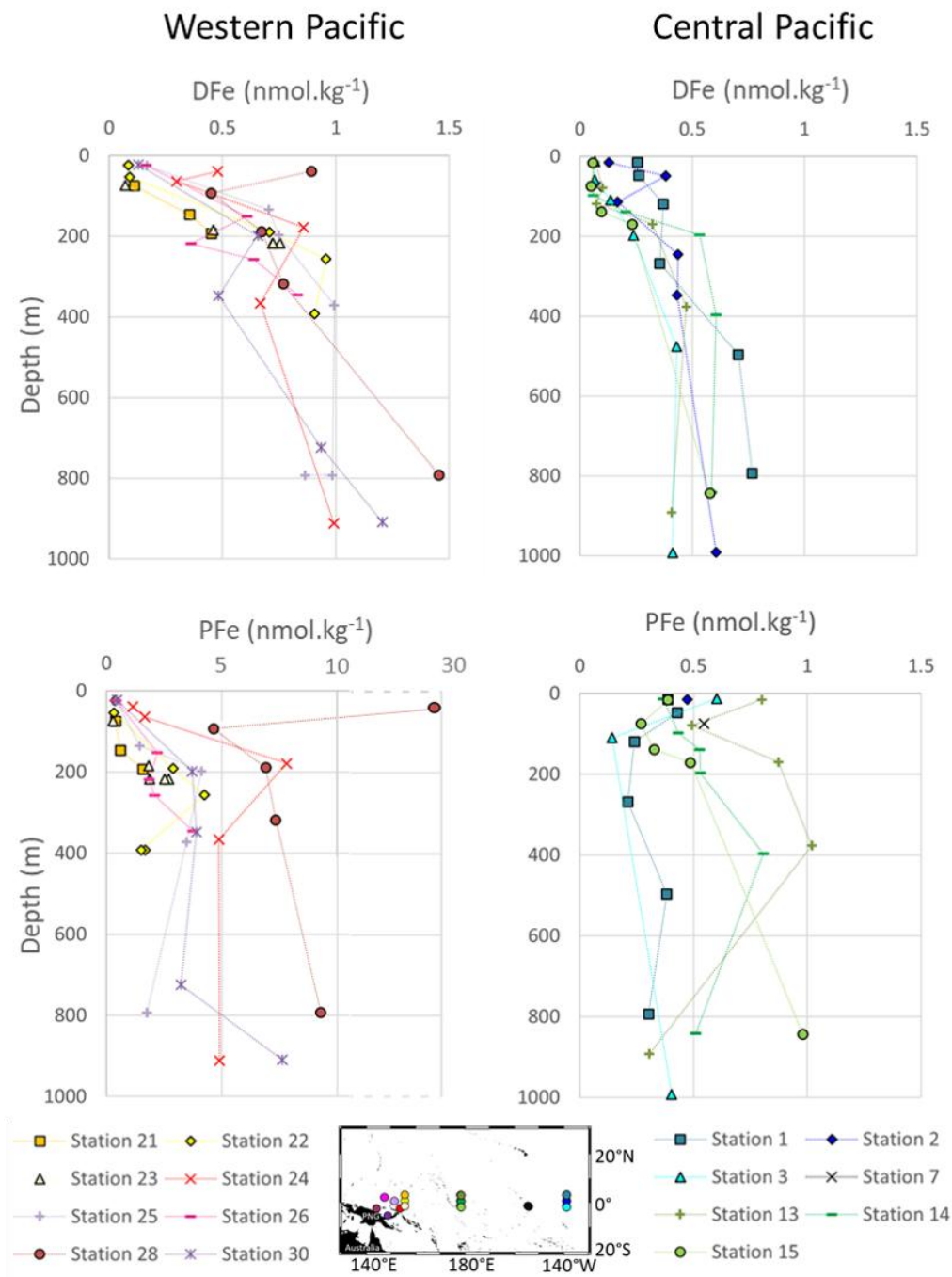
GoFlo bottle	Depth (m)	θ (°C)	Salinity	O ₂ (μmol. kg ⁻¹)	σ _θ (kg. m ⁻³)	Water mass	DFe (nmol. kg ⁻¹)	δ ⁵⁶ DFe (‰)	δ ⁵⁶ DFe U95 (‰)	PFe (nmol. kg ⁻¹)	δ ⁵⁶ PFe (‰)	δ ⁵⁶ PFe U95 (‰)
STATION 1 (1.6°N 140.0°W, cast TM3, 25 August 2006, bottom depth: 4364 m)												
12	15	26.5	35.05	204	22.93	ESW	0.26	+0.43	0.08	0.39	+0.06	0.07
10	48	26.4	35.09	202	22.98	ESW (Chloro. Max.)	0.26	+0.32	0.07	0.43	+0.25	0.07
8	119	19.2	34.79	81	24.82	NPEW	0.37	+0.28	0.08	0.24	+0.23	0.07
6	268	12.3	34.87	43	26.43	WSPCW	0.36	-0.19	0.11	0.21	+0.06	0.07
4	497	8.8	34.65	(°) 23	26.88	WSPCW	0.71	-0.22	0.09	0.38	+0.12	0.07
2	794	5.3	34.54	(°) 87	27.28	SEqIW	0.77	+0.40	0.07	0.30	-0.11	0.07
STATION 2 (0.0°N 140.0°W, cast TM9, 26 August 2006, bottom depth: 4333 m)												
12	15	26.5	35.33	201	23.13	ESW	0.13	+0.19	0.07	0.47	+0.19	0.07
10	49	26.2	35.36	188	23.23	ESW (Chloro. Max.)	0.38	+0.14	0.09	—	—	—
8	114	24.3	35.59	143	24.00	SPEW	0.17	+0.25	0.07	—	—	—
6	246	13.0	34.93	98	26.34	WSPCW	0.44	+0.29	0.07	—	—	—
4	348	11.4	34.82	(°) 24	26.57	WSPCW	0.43	-0.10	0.07	—	—	—
2	992	4.6	34.55	(°) 86	27.37	SEqIW	0.61	+0.11	0.07	—	—	—
STATION 3 (2.0°S 139.6°W, cast TM11, 27 August 2006, bottom depth: 4257 m)												
12	13	26.9	35.51	203	23.13	ESW	0.07	—	—	0.60	+0.41	0.07
10	59	26.9	35.51	205	23.14	ESW (Chloro. Max.)	0.06	+0.31	0.07	—	—	—
8	110	20.3	35.76	167	25.25	SPTW	0.14	+0.30	0.12	0.14	+0.33	0.07
7	198	12.8	34.93	25	26.37	WSPCW	0.24	-0.06	0.07	—	—	—
4	476	9.0	34.67	(°) 36	26.87	SEqIW	0.43	+0.14	0.07	—	—	—
1-2	993	4.5	34.55	(°) 91	27.37	SEqIW	0.41	+0.35	0.07	0.40	+0.15	0.08
STATION 7 (2.1°S 155.1°W, cast TM16, 02 September 2006, bottom depth: 4992 m)												

11	75	27.9	35.61	196	22.87	ESW (Chloro. Max.)	0.07	—	—	0.55	+0.22	0.07
STATION 13 (2.0°N 179.6°W, cast TM25, 10 September 2006, bottom depth: 5218 m)												
12	15	30.3	34.43	195	21.20	ESW	0.07	+0.79	0.07	0.80	-0.04	0.08
10	79	29.2	35.32	184	22.23	ESW (Chloro. Max.)	0.10	+0.35	0.07	0.49	+0.26	0.11
8	119	28.2	35.49	137	22.69	ESW	0.07	+0.72	0.07	—	—	—
7	170	13.8	34.69	134	25.98	NPCW	0.32	+0.30	0.08	0.87	+0.12	0.10
4	377	10.3	34.75	(*) 68	26.70	WSPCW	0.47	+0.35	0.07	1.02	+0.12	0.12
2	892	5.1	34.54	97	27.30	SEqIW	0.41	+0.25	0.07	0.31	—	—
STATION 14 (0.0°N 180°E, cast TM28, 11 September 2006, bottom depth: 5260 m) (+)												
12	14	30.4	34.67	201	21.35	ESW	0.06	—	—	0.37	+0.27	0.07
10	98	29.4	35.39	186	22.22	ESW (Chloro. Max.)	0.06	+0.58	0.07	0.43	+0.43	0.09
8	139	22.6	35.56	137	24.48	SPEW	0.20	+0.31	0.08	0.53	+0.13	0.09
6	197	14.9	34.86	140	25.88	WSPCW	0.53	+0.40	0.12	0.53	+0.40	0.07
4	397	9.8	34.71	64	26.76	WSPCW	0.61	+0.01	0.07	0.81	+0.15	0.11
2	842	5.3	34.54	82	27.27	SEqIW	0.59	+0.22	0.08	0.51	+0.28	0.10
STATION 15 (2.0°S 180.0°E, cast TM30, 12 September 2006, bottom depth: 5390 m)												
12	16	30.2	34.49	206	21.27	ESW	0.06	+0.55	0.07	0.39	+0.27	0.07
10	75	29.3	35.49	199	22.32	ESW (Chloro. Max.)	0.05	—	—	0.27	+0.30	0.07
8	139	24.2	35.98	134	24.31	SPTW	0.10	+0.43	0.07	0.33	+0.23	0.12
6	171	16.4	35.35	133	25.93	WSPCW	0.23	+0.20	0.07	0.49	+0.12	0.11
2	844	5.3	34.53	99	27.27	SEqIW	0.58	+0.32	0.07	0.98	-0.05	0.10
STATION 21 (2.0°N 156.0°E, cast TM40, 20 September 2006, bottom depth: 2587 m)												
10	75	28.1	35.37	158	22.65	ESW (Chloro. Max.)	0.11	—	—	0.41	+0.18	0.14
8	147	24.4	35.48	129	23.89	SPEW	0.36	+0.40	0.08	0.60	-0.05	0.07
7	194	12.0	34.58	124	26.25	NPCW	0.45	+0.16	0.07	1.59	+0.05	0.07
STATION 22 (0.2°N 156.0°E, cast TM43, 21 September 2006, bottom depth: 2049 m)												
12	24	29.7	33.91	200	21.00	ESW	0.09	—	—	0.39	+0.19	0.07
10	54	28.6	34.89	195	22.12	ESW (Chloro. Max.)	0.09	—	—	0.32	+0.22	0.07
8	191	18.2	35.35	143	25.49	SPEW	0.71	+0.48	0.08	2.89	+0.00	0.07
6	257	12.2	34.82	134	26.41	WSPCW	0.96	+0.40	0.07	4.26	+0.02	0.07
4	393	9.3	34.68	(*) 101	26.82	SAMW	—	—	—	1.51	+0.01	0.12
3	393	9.3	34.68	(*) 101	26.82	SAMW	0.91	+0.25	0.07	1.68	+0.05	0.15
STATION 23 (1.2°S 155.6°E, cast TM45, 22 September 2006, bottom depth: 1997 m)												
10	74	28.2	35.35	(*) 183	22.60	ESW (Chloro. Max.)	0.07	+0.26	0.09	0.29	+0.14	0.11
8	185	18.4	35.50	(*) 138	25.56	SPEW	0.46	+0.32	0.09	1.83	-0.03	0.14
6	218	13.6	35.08	(*) 137	26.34	WSPCW	0.72	+0.29	0.07	1.87	+0.04	0.07
5	218	13.6	35.08	(*) 137	26.34	WSPCW	0.72	+0.30	0.11	2.52	-0.01	0.13

4	218	13.6	35.08	(*) 137	26.34	WSPCW	0.75	+0.22	0.07	2.70	+0.03	0.12
STATION 24 (3.2°S 152.3°E, cast TM47, 23 September 2006, bottom depth: 1669 m) (°)												
11	39	28.7	34.56	199	21.83	ESW	0.48	-0.03	0.07	1.15	+0.13	0.14
9	64	27.4	34.74	196	22.38	ESW (Chloro. Max.)	0.30	+0.20	0.07	1.66	+0.01	0.16
7	179	19.9	35.57	133	25.22	SPEW	0.86	-0.03	0.07	7.81	-0.48	0.11
5	367	10.5	34.78	(*) 143	26.70	WSPCW	0.67	+0.27	0.08	4.87	-0.03	0.12
2	912	4.6	34.52	141	27.34	AAIW	0.99	+0.34	0.07	4.91	+0.00	0.10
STATION 25 (0°N 149.3°E, cast TM50, 25 September 2006, bottom depth: 3364 m)												
11	25	29.4	33.95	215	21.14	ESW	0.17	—	—	0.44	+0.25	0.09
9	135	21.9	35.69	133	24.79	SPEW	0.70	+0.03	0.13	1.44	-0.52	0.10
6	198	15.6	35.20	136	26.00	WSPCW	0.75	+0.38	0.14	4.12	+0.02	0.07
5	372	10.3	34.75	(*) 126	26.71	SAMW	0.99	—	—	3.48	+0.00	0.07
3	793	5.5	34.53	(*) 103	27.24	SEqIW	0.98	+0.13	0.07	1.76	-0.06	0.07
2	793	5.5	34.53	(*) 103	27.24	SEqIW	0.87	—	—	1.77	-0.05	0.07
STATION 26 (1.6°N 145.0°E, cast TM52, 26 September 2006, bottom depth: 4490 m)												
11	24	28.8	34.03	200	21.40	ESW	0.16	—	—	0.42	—	—
8	152	20.0	35.41	135	25.08	SPEW	0.61	—	—	2.20	+0.01	0.07
6	219	16.4	34.77	(*) 144	25.48	NPEW	0.36	—	—	1.85	+0.12	0.07
5	258	10.4	34.52	(*) 111	26.51	NPCW	0.64	+0.20	0.07	2.09	+0.04	0.07
3	346	9.4	34.67	(*) 127	26.79	WSPCW	0.83	—	—	3.76	+0.02	0.07
STATION 28 (3.4°S 143.9°E, cast TM56, 28 September 2006, bottom depth: 2256 m) (+) (°)												
10	39	27.5	34.70	196.6	22.32	ESW	0.89	+0.53	0.07	29.45	+0.04	0.09
8	94	26.5	34.85	180.9	22.77	ESW (Chloro. Max.)	0.45	+0.40	0.10	4.64	+0.01	0.07
7	189	19.1	35.45	145	25.33	SPEW	0.67	+0.43	0.11	6.91	+0.29	0.07
5	319	13.8	35.09	154	26.31	WSPCW	0.77	+0.29	0.07	7.34	+0.04	0.07
2	793	5.5	34.50	151	27.22	AAIW	1.46	+0.06	0.07	9.29	-0.03	0.10
STATION 30 (5.6°S 147.4°E, cast TM61, 30 September 2006, bottom depth: 1040 m) (°)												
10	23	27.3	34.76	(*) 200	22.44	ESW	0.13	—	—	0.45	+0.30	0.11
7	199	18.7	35.53	(*) 144	25.49	SPEW	0.65	+0.41	0.12	3.72	+0.17	0.07
6	348	11.8	34.92	(*) 162	26.57	WSPCW	0.48	+0.31	0.07	3.90	+0.20	0.07
3	724	5.9	34.48	(*) 166	27.15	AAIW	0.94	+0.44	0.12	3.23	+0.01	0.07
2	909	4.6	34.51	(*) 143	27.33	AAIW	1.21	—	—	7.62	-0.03	0.07

266

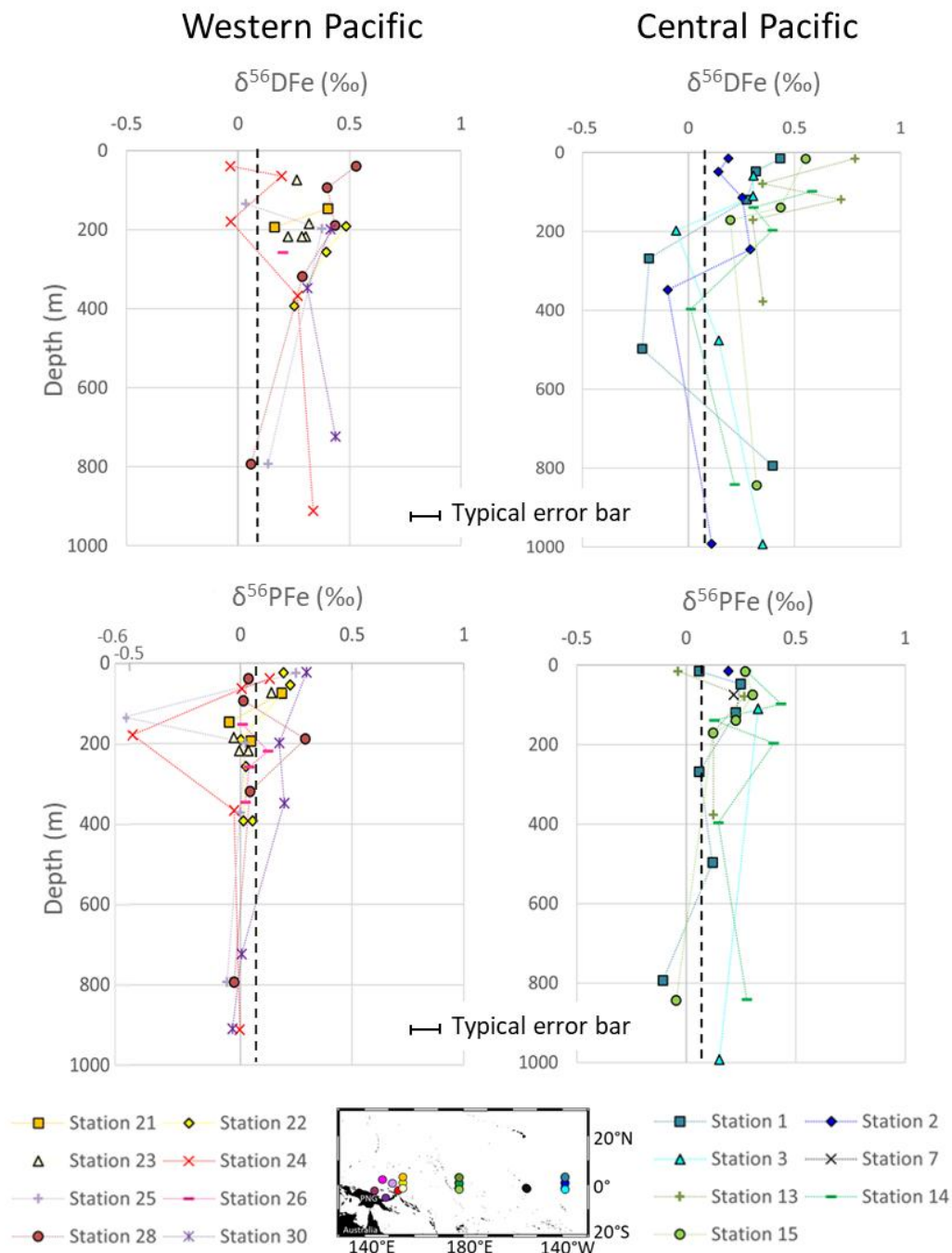
267 Two distinct groups of stations emerge from these observations. These are the western
268 equatorial Pacific and central equatorial Pacific. In the western equatorial Pacific, PFe
269 concentrations were significantly higher, approximately seven times larger, than typical open
270 ocean values. This group includes stations 21, 22, 23, 24, 25, 26, 28 and 30. In the central
271 equatorial Pacific, PFe concentrations were mostly typical of open ocean values. This group
272 includes stations 1, 2, 3, 7, 13, 14 and 15. Data for both areas are shown in Figures 3 and 4.



273

274 Figure 3. Profiles of concentrations of DFe and PFe in nmol.kg⁻¹ in the western equatorial and
 275 central equatorial Pacific. For each station, the error bars are smaller than the symbols for Fe
 276 concentrations: on average 8 % for DFe and 4 % for PFe. Stations 14 and 28 were
 277 previously published by Radic et al. (2011) and stations 24, 28 and 30 by Labatut et al. (2014).
 278 The x-axis is broken to show all PFe concentrations from western equatorial Pacific stations.

279



280

281 Figure 4. $\delta^{56}\text{DFe}$ and $\delta^{56}\text{PFe}$ profiles in the western equatorial and central equatorial Pacific.
 282 The black dashed line indicates the crustal value, +0.07 ‰ (Poitrasson, 2006). Individual error
 283 bars are not shown for clarity, but typical uncertainty (± 0.07 ‰) is indicated by the scale bar.

284

285 4.1. IRON CONCENTRATIONS

286 DFe and PFe concentrations ranged from 0.05 to 1.46 nmol.kg^{-1} and from 0.14 to 29.45
 287 nmol.kg^{-1} , respectively.

288 A few common features in Fe concentration profiles can be identified across stations
 289 from the surface down to 1 000 m. i) With the exception of station 28 located near the mouth
 290 of the Sepik River, lowest concentrations were found near the surface, mostly in the chlorophyll

291 maximum layer, where biological uptake depletes the concentration of bioavailable Fe. ii) From
292 the surface to 200 m depth, Fe concentrations tended to increase. Deeper than 200 m, the
293 profiles became more variable, with no uniform trend across stations. iii) Stations 3, 13, 14 and
294 15 displayed typical open ocean, nutrient like, DFe profiles. iv) The particulate iron (PFe)
295 fraction predominated over the dissolved fraction (DFe), accounting on average for 80 %
296 mol.mol^{-1} of total iron (TFe) at western equatorial Pacific stations (140°E–156°E) and 66 %
297 mol.mol^{-1} at central equatorial Pacific stations (180°E–140°W) (Figure A1).

298 Slemons et al. (2010, 2012) measured DFe and PFe concentrations by FIA during the
299 same cruise. All data were of the same order of magnitude and ranged similarly. However, our
300 data were almost systematically slightly lower (with a mean difference of $0.35 \pm 0.44 \text{ nmol.kg}^{-1}$
301 1 for DFe and $0.35 \pm 0.90 \text{ nmol.kg}^{-1}$ for PFe). In addition, EUCFe DFe and PFe concentration
302 data are in good agreement with data published in the same area (John et al., 2018; Marsay et
303 al., 2018b; Zheng and Sohrin, 2019; Cohen et al., 2021; Sarthou et al., 2025).

304

305 4.2. IRON ISOTOPIC COMPOSITIONS

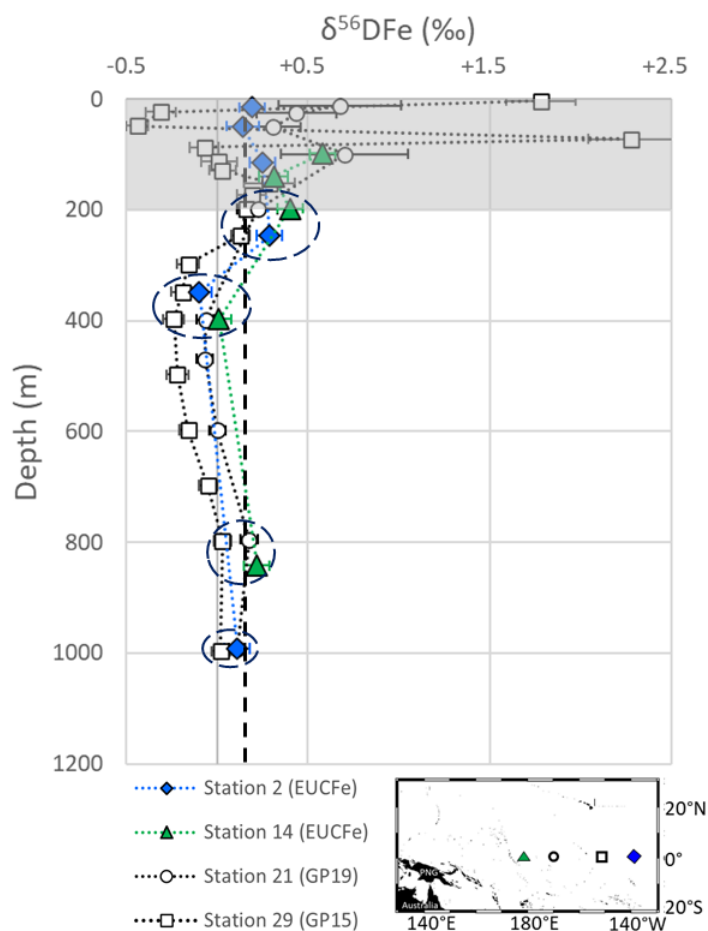
306 The isotopic signatures of dissolved ($\delta^{56}\text{DFe}$) and particulate Fe ($\delta^{56}\text{PFe}$) ranged
307 from -0.22 to +0.79 ‰ and -0.52 to +0.43 ‰, respectively (Figure 4).

308 Across all stations, 85 % of the samples had exhibited isotopic compositions of
309 dissolved iron ($\delta^{56}\text{DFe}$) higher than the upper continental crust (UCC) reference value of
310 +0.07 ‰ (Poitrasson, 2006). $\delta^{56}\text{DFe}$ of western equatorial Pacific stations ranged from -0.03 ‰
311 to +0.53 ‰, with an average of $+0.28 \pm 0.30 \text{ ‰}$ (2SD, n=27) and showed no systematic
312 variation with depth or location. At the central equatorial Pacific stations, $\delta^{56}\text{DFe}$ ranged from
313 -0.22 ‰ to +0.79 ‰, with an average of $+0.27 \pm 0.45 \text{ ‰}$ (2SD, n=32). The surface layer
314 exhibited relatively heavy isotopic signatures (around +0.5 ‰), which generally decreased with
315 depth, reaching values around -0.2 ‰ at approximately 400 m. Below this depth, between 800
316 and 1 000 m, $\delta^{56}\text{DFe}$ values increased again, to +0.4 ‰.

317 The isotopic compositions of particulate iron ($\delta^{56}\text{PFe}$) at the western equatorial Pacific
318 stations, $+0.03 \pm 0.32 \text{ ‰}$ (2SD, n=39) on average, were remarkably homogeneous and
319 remained close to the upper continental crust (UCC) value, except for two samples from stations
320 24 and 25. At the central equatorial Pacific stations, $\delta^{56}\text{PFe}$ were slightly more variable, from -
321 0.11 to +0.43 ‰ (with an average of $+0.19 \pm 0.27 \text{ ‰}$, 2SD, n=26), and 81 % of the samples
322 were heavier relative to the UCC.

323 EUCFe data can also be compared with ~~two~~three nearby cruises: GEOTRACES GP16
324 (2013), a zonal cruise along 10°S, from 75°W to 155°W, GEOTRACES GP15 (2018), a
325 meridional section along 150°W with one station located at the equator and GEOTRACES
326 GP19 (2015), a meridional section along 170°W with one station located at the equator (Figure
327 1). In the equatorial Pacific area, the circulation is highly zonal, and previous studies have
328 shown that the water mass geochemistry at 12°S is not directly linked to that of the equatorial
329 band (Lacan and Jeandel, 2001). This prevents the use of GP16 data and limits that of GP15
330 and GP19 to ~~its~~ their equatorial stations (stations 29 and 21, respectively). These GP15 and
331 GP19 Fe isotope data have not yet been published but are available in GEOTRACES
332 Intermediate Data Product 2021+25 (GEOTRACES Intermediate Data Product Group, 20235).
333 Figure 5 displays the GP15 station 29 and GP19 station 21 $\delta^{56}\text{DFe}$ profiles with the closest
334 equatorial EUCFe stations, stations 2 and 14 (EUCFe station 7 is excluded from this comparison
335 because it only reports a single data point at 75 m). Given the nine year lag between the two
336 cruises, and the thousand km between the stations, the upper 200 m are excluded from this

337 comparison due to potential variabilities. At four depths, approximately 200, 400, 800 and 1 000
 338 m, $\delta^{56}\text{DFe}$ data from the [twothree](#) cruises can be compared (Figure 5). These are in excellent
 339 agreement. No $\delta^{56}\text{PFe}$ data have been reported for [GP15](#) and [GP19](#).



340
 341 Figure 5. Comparison of $\delta^{56}\text{DFe}$ values from the EUCFe, [GP15](#) and [GP19](#) cruises. The upper
 342 200 m, shaded in gray, are excluded from the comparison. The dashed ellipses show the 4
 343 depths where comparison can be made for $\delta^{56}\text{DFe}$ values. Please note that at 1000 m, values
 344 from stations 2, 21 and 29 are close, making station 21 less visible. The black dashed line
 345 indicates the crustal value. The [GP15](#) cruise data were produced by M. Sieber and T. Conway,
 346 and the [GP19](#) cruise data were produced by T. Conway, M. Sieber, and D. Vance; both datasets
 347 are available in the [GEOTRACES](#) Data product ([GEOTRACES](#) Intermediate Data Product
 348 Group, 20235).

349
 350 **5. DISCUSSION**

351
 352 **5.1. INFLUENCE OF EXTERNAL IRON INPUTS IN THE WESTERN EQUATORIAL PACIFIC**

353 Fe concentrations throughout the entire water column in the western equatorial Pacific
 354 were approximately twice as high for DFe ($0.63 \text{ nmol.kg}^{-1}$ compared to $0.30 \text{ nmol.kg}^{-1}$, on
 355 average) and approximately seven times higher for PFe ($3.58 \text{ nmol.kg}^{-1}$ compared to 0.49
 356 nmol.kg^{-1} , on average) at the western equatorial Pacific stations compared relative to the central
 357 equatorial Pacific stations throughout the entire water column. The particulate Fe (PFe) fraction

358 dominated total Fe (TFe), particularly in the western equatorial Pacific stations, where PFe/TFe
359 ratios ranged from 63 to 97 % mol.mol⁻¹ (Figure A1). These patterns were documented
360 previously in several studies, and attributed to lithogenic inputs from terrestrial sources, with
361 occasional hydrothermal contributions and minimal input from atmospheric sources (Milliman,
362 1995; Kineke et al., 2000; Mackey et al., 2002; Slemmons et al., 2010; Radic et al., 2011; Labatut
363 et al., 2014).

364 A box model (Figure 6) for the region defined by (133°E–177°W, 9°S–15°N) was used
365 to investigate the relative importance of possible PFe sources leading to these high
366 concentrations. ~~It included~~The model includes PFe transported by oceanic currents,
367 atmospheric deposition and delivered by rivers (notably the Sepik River, with potential
368 deposition to and resuspension from ~~the~~ sediments). Particle settling within the water column
369 and hydrothermal sources were neglected (Figure 6).

370 The transport of water masses in this area, from the surface to a depth of 1 000 m, was estimated
371 at $19.4 \pm 0.418.7$ Sv (1SD), based on the flow in Vitiaz Strait during the Austral winter (i.e., the
372 same period as the EUCFe cruise) (Germineaud et al., 2016). The incoming water is assumed
373 to carry a typical open ocean PFe concentration (average value for the upper 1000 m of the
374 water column, station 36, GP16 cruise) of 0.15 ± 0.08 nmol.kg⁻¹ (1SD) (Marsay et al., 2018)
375 ~~0.5 nmol.kg⁻¹ (Tillette et al., 2022)~~, prior to enrichment within the study area. The flux of PFe
376 transported by water masses into this area, calculated as the product of these two quantities, is
377 Flux PFe_{SW in} = 14.5×10^6 g ~~45 tons~~(PFe).day⁻¹. The average PFe concentration in this area
378 (stations 21 to 30) ~~was 3.6~~ ranged between 2.9 and 3.8 nmol.kg⁻¹ depending on the calculation
379 method chosen (Table A1). The fluxes derived from these concentrations will be given as a
380 range. This leads to a PFe flux transported out of the area by water masses, Flux PFe_{SW out}, ~~= of~~
381 ~~between~~ 272×10^6 and 357×10^6 g ~~326 tons~~(PFe).day⁻¹ (~~3.6 nmol.kg⁻¹ concentration multiplied~~
382 ~~by 19.4-18.7 Sv~~). In a steady state model, where inputs are balanced by outputs, one or more
383 sources must be contributing approximately between 258×10^6 and 342×10^6 g~~281~~
384 ~~tons~~(PFe).day⁻¹ to this area.

385 Particulate iron atmospheric deposition was estimated using the Fe concentration in aerosols
386 over this region, measured during the same cruise at 3.01 ng.m⁻³ (Camin et al., 2025), multiplied
387 by a bulk aerosol deposition velocity ~~typical aerosol deposition velocity of 1,000 m.day⁻¹~~
388 ~~(Shelley et al., 2017)~~. ~~Using~~The deposition area shown in Figure 6, chosen as representative
389 of this region of elevated PFe concentrations, ~~and covering~~ covers approximately 1.54×10^7
390 km² (the box model surface area of 1.6×10^7 km² minus the New Guinea land area of
391 0.08×10^7 km²; Baldacchino et al., 2024). The bulk aerosol deposition velocity, denoted V_b
392 (m.day⁻¹), includes both wet and dry deposition. It can be calculated from the precipitation rate
393 (mm.day⁻¹) according to the formula from Kadko et al., 2020, recently updated by He et al.,
394 2025, who used ⁷Be as a proxy for atmospheric deposition:

$$395 \quad V_b = 413 \pm 22 \times \text{Precipitation Rate} + 1069 \pm 71 \quad (\text{Equation 2})$$

396 To estimate the precipitation rate, we used the NASA Giovanni data product TRMM to
397 determine the mean daily precipitation rate over the entire region considered in the box model
398 from September 20 to 30, 2006. The mean value was 11.4 ± 6.6 mm.day⁻¹ (2SD) (Table A2).
399 Applying Equation 2, the bulk aerosol deposition velocity is therefore $5\,777$ m.day⁻¹. ~~The~~
400 resulting atmospheric PFe deposition flux was Flux PFe_{aerosol} = 268×10^6 g ~~49 tons~~(PFe).day⁻¹.
401 This estimate accounts for ~~only~~ between 78 and 104 ~~45~~ % of the required external sources (Table
402 A1). However as discussed below, this PFe atmospheric deposition flux is orders of magnitudes
403 lower than that delivered by rivers. ~~Another external source to consider is sedimentary PFe flux~~
404 ~~delivered by rivers.~~

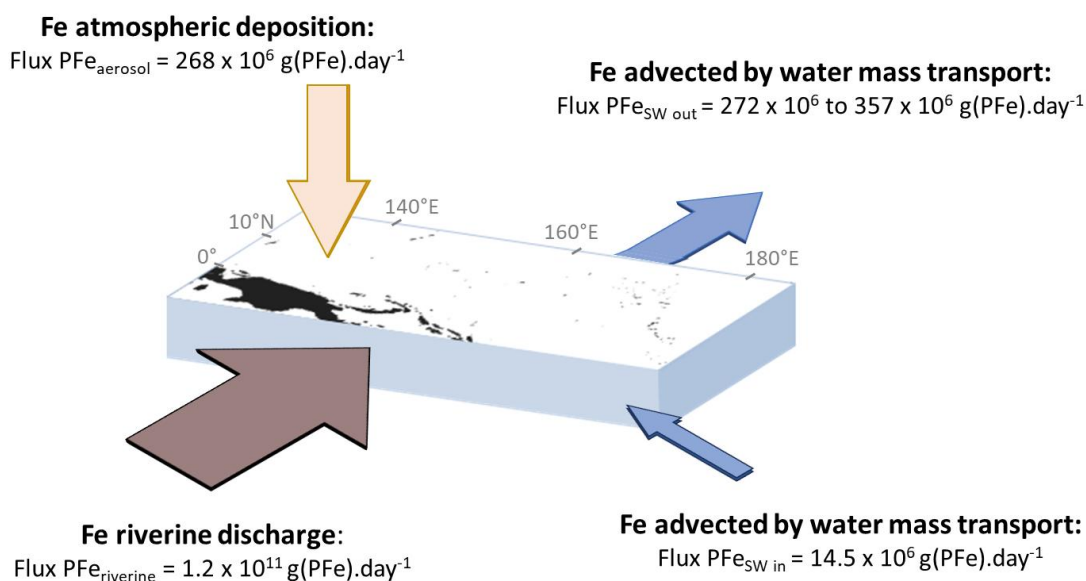
405 ~~Assuming steady state, mass conservation for this model implies:~~

406
$$\text{Flux PFe}_{\text{SW in}} + \text{Flux PFe}_{\text{aerosol}} + \text{Flux PFe}_{\text{sediment}} = \text{Flux PFe}_{\text{SW out}} \quad (\text{Equation 2})$$

407 ~~Taking into account the above estimates for Flux PFe_{SW in}, Flux PFe_{SW out}, and Flux PFe_{aerosol},~~
 408 ~~we obtain PFe_{sediments} = 232 tons(PFe).day⁻¹, for the sedimentary PFe flux delivered by rivers and~~
 409 ~~reaching the western equatorial Pacific area.~~

410 Papua New Guinea accounts for 8 to 10 % of the global export of sediment export to the ocean
 411 (1.7×10^{17} gtons(sediment).year⁻¹) (Milliman et al., 1999)., with the Sepik River and other
 412 northern rivers of PNG discharging 8.6×10^{14} gtons(sediment).year⁻¹ to this study area
 413 (Milliman et al., 1999). Assuming that Fe amounts to 5 % w.w⁻¹ of the sediment discharge, (the
 414 upper continental crust (UCC) value from Rudnick and Gao, 2014), the estimated riverine
 415 discharge of PFe to the western equatorial Pacific is 4.3×10^{13} gtons(PFe).year⁻¹, i.e., 1.2×10^{11}
 416 gtons(PFe).day⁻¹. This estimate accounts for between 35,064 and 46,556 % of the required
 417 external sources (Table A1).

418 ~~A very small fraction, 0.2 %, of this flux would therefore be sufficient to account for the~~
 419 ~~necessary 232 tons(PFe).day⁻¹. This confirms that the riverine sediment discharge is, by far, the~~
 420 ~~predominant source of PFe to this area. Thus, the riverine PFe flux is 448-fold larger than the~~
 421 ~~atmospheric PFe flux. This flux comparison argues in favor of a contribution dominated by~~
 422 ~~input from rivers. Isotopic signatures provide an additional constraint and also support a riverine~~
 423 ~~source, as the $\delta^{56}\text{PFe}$ values are close to crustal values in this region (Table 2 and Figure 4),~~
 424 ~~whereas aerosols exhibit a heavier isotopic signature, around +0.3 ‰ (Camin et al., 2025).~~



425
 426 Figure 6. Box model describing PFe inputs and output to the western equatorial Pacific region.
 427 Note that all of the external sources end up in seawater. Some are removed to the sediments.

428 Regarding riverine particles, the question of their transport mechanism over such a
 429 distance from the coast (~1 200 km) arises. The Sepik River and other northern rivers of PNG
 430 deliver large sediment loads to the coastal ocean due to factors including intense rainfall from
 431 the Inter-Tropical Convergence Zone, a narrow shelf associated with the active margin, the
 432 sediment erodibility (geology, human activities) and tectonism (seismic and volcanic activity,
 433 relief) (Milliman and Syvitski, 1992). Lithogenic iron (Fe) observed at the western equatorial
 434 Pacific stations can be due to direct fluvial inputs, resuspended sediments, isopycnal plumes,
 435 and hyperpycnal flows (Kineke et al., 2000; Mackey et al., 2002; Kuehl et al., 2004; Renagi et
 436 al., 2010; Slemons et al., 2010). These processes can transport Fe seaward across the slope
 437 (Kineke et al., 2000; Kuehl et al., 2004; Renagi et al., 2010). These lithogenic inputs, leading
 438 to very significant PFe excess compared to open ocean values, extend throughout the sampled

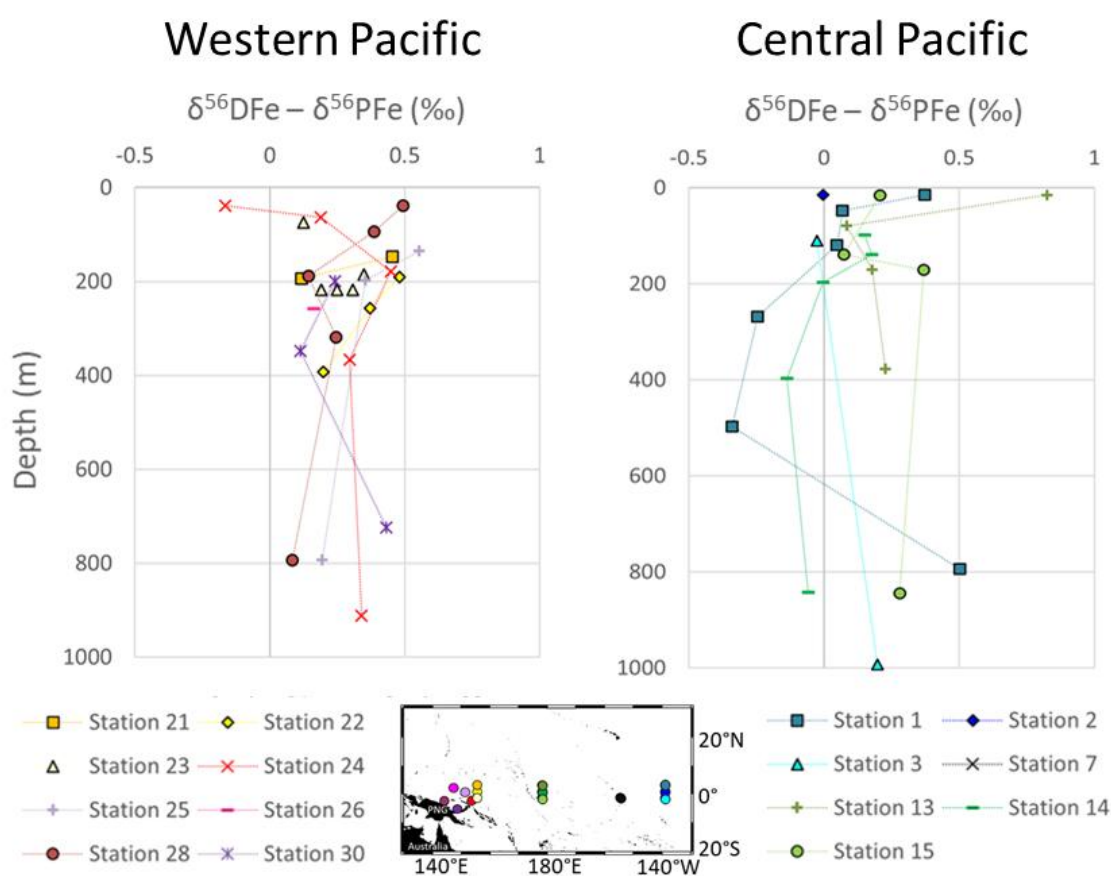
439 water column (0 – 1 000 m) at all stations ~~located~~ in the western equatorial Pacific. Therefore,
440 we discuss these data below as a whole, without distinguishing between different water masses
441 or currents.

442 At the western equatorial Pacific stations, PFe isotopic compositions are close to the
443 UCC reference value, supporting ~~the~~ predominantly lithogenic origin discussed above (Table
444 2 and Figure 4). Only two samples, from stations 24 and 25, exhibit near-zero $\delta^{56}\text{DFe}$ and
445 $\delta^{56}\text{PFe}$ values close to -0.5 ‰, likely reflecting a hydrothermal contribution, as previously
446 suggested by Labatut et al. (2014) for station 24. Northeastern PNG is an active margin with
447 hydrothermal activity (Auzende et al., 2000) with shallow sources able to supply EUC via the
448 NICU (Mackey et al., 2002).

449 The isotopic difference between dissolved and particulate Fe, $\Delta^{56}\text{Fe}_{\text{DFe-PFe}}$, is shown in
450 Figure 7. Except for one data point at the surface this difference is ~~consistently~~~~systematically~~
451 positive, i.e., DFe is systematically heavier than PFe. This is true for 26 ~~data points~~
452 ~~data points~~, including the two data points discussed above with significantly different $\delta^{56}\text{PFe}$
453 values (attributed to hydrothermal influence). On average this difference is $\Delta^{56}\text{Fe}_{\text{DFe-PFe}} = +0.27$
454 ± 0.32 ‰ (2SD, n=27). This systematic difference suggests a mechanistic link between
455 particulate and dissolved Fe pools, associated ~~with~~~~the~~ an isotopic fractionation. A kinetic
456 isotopic fractionation associated ~~with~~~~the~~ an unidirectional reaction would lead to a reaction
457 product isotopically lighter than the reactant. In such a hypothesis, PFe being lighter than DFe,
458 this would imply that PFe is produced from DFe (for instance ~~by~~~~through~~ precipitation). This is
459 totally unlikely given the predominance of lithogenic PFe sources in this area. We ~~can~~
460 exclude the hypothesis of a kinetic fractionation and conclude that there is an equilibrium
461 isotopic fractionation between PFe and DFe. Equilibrium fractionation implies co-occurrence
462 of chemical fluxes from both phases toward the other. ~~This implies the occurrence of a~~
463 ~~permanent and reversible exchange between dissolved and particulate Fe phases.~~ In addition,
464 because DFe is heavier than PFe, the processes responsible for the flux from the particulate to
465 the dissolved phase cannot be associated with an Fe reduction process (that would ~~have~~
466 ~~produce~~~~d~~ lighter DFe, (Criss, 1999)). This is consistent with the oxygenated water column in
467 this region (Table 2). The PFe to DFe flux is therefore a non-reductive release of dissolved Fe,
468 a process named non-reductive dissolution, NRD, by Radic et al. (2011). The term NRD can
469 refer to dissolution, as well as to other type of processes from the particulate to the dissolved
470 phase, such as desorption ~~processes~~. This non-reductive release of dissolved Fe probably
471 reflects processes similar to the reversible scavenging process proposed for Th or rare earth
472 elements (REE) (Bacon and Anderson, 1982; Nozaki et al., 1987; Nozaki and Alibo, 2003).
473 These conclusions have ~~already~~ been ~~previously~~ proposed ~~in previous studies~~ for stations 24,
474 28 and 30 (Radic et al., 2011; Labatut et al., 2014). The addition of data from five additional
475 western stations reinforces the conclusions drawn from earlier studies and extends the
476 geographic scope of these findings eastward beyond the Bismarck Sea, ~~to~~~~reaching~~ as far as
477 156°E. This confirms the significant role of lithogenic inputs from PNG on the biogeochemistry
478 of the area. These processes govern particulate - dissolved interactions at least up to 1 200 km
479 from the source, within the upper 1 000 m of the water column.

480 The non-reductive release of dissolved iron, NRD, at the sediment / water column interface has
481 now been observed in numerous studies as a significant external DFe source. These include the
482 western Pacific (Radic et al., 2011; Labatut et al., 2014; this study), the northwest Atlantic
483 (Conway and John, 2014), the northeast Atlantic (Klar et al., 2018), the southeast Atlantic
484 (Conway et al., 2016), the Southern Ocean (Abadie et al., 2017; Tian et al., 2023) and in the
485 southeast Pacific (John et al., 2018). In the water column, exchange fluxes between particulate
486 and dissolved phases, including non-reductive release of dissolved iron from the particles, have
487 also been proposed in several other studies (Radic et al., 2011; Abadie et al., 2017; Fitzsimmons
488 et al., 2017; John et al., 2018). In all cases, at the sediment/seawater interface and within the
489 water column, the exact processes involved remain unclear. Desorption and ligand-promoted

490 dissolution have notably been suggested (Abadie et al., 2017; John et al., 2018; Homoky et al.,
 491 2021). Additionally, direct comparison of DFe and total PFe isotopic compositions has inherent
 492 limitations, as it does not allow us to study the distinct processes related to different PFe phases
 493 (lithogenic, biogenic, Fe oxyhydroxides). Those PFe phases are likely not equally involved in
 494 particulate - dissolved exchanges. Nevertheless, our analytical approach employs total digestion
 495 to guarantee the absence of artifactual isotopic fractionation. The regional geochemical
 496 characteristics establish that excess PFe is predominantly lithogenic (Figure 6), with excess
 497 DFe correspondingly derived from this source. Although lithogenic iron is conventionally
 498 considered refractory, neodymium isotope studies have shown that lithogenic phases do
 499 dissolve, even if in small proportions (Lacan and Jeandel, 2005; Rousseau et al., 2015). The
 500 excess DFe in the area, from 0.30 to 0.63 nmol.kg⁻¹, affects 19.4 Sv (Germineaud et al., 2016).
 501 This leads to a required flux of ~540 g(DFe).s⁻¹. The riverine PFe discharge to this area is about
 502 1.2 x 10¹¹ g(PFe).day⁻¹. Therefore, the dissolution of only 0.04 % of the PFe discharge would
 503 be sufficient to account for the observed DFe increase. This very low dissolution rate makes it
 504 entirely plausible that the excess DFe originates from the dissolution of lithogenic PFe.



505
 506 Figure 7. Differences between the dissolved and particulate of iron isotopic compositions
 507 ($\delta^{56}\text{DFe} - \delta^{56}\text{PFe}$) from the surface to 1 000 m depth in the western equatorial and central
 508 equatorial Pacific.

509
 510 **5.2. IRON SOURCES AND BIOGEOCHEMICAL DYNAMICS IN THE CENTRAL EQUATORIAL**
 511 **PACIFIC**

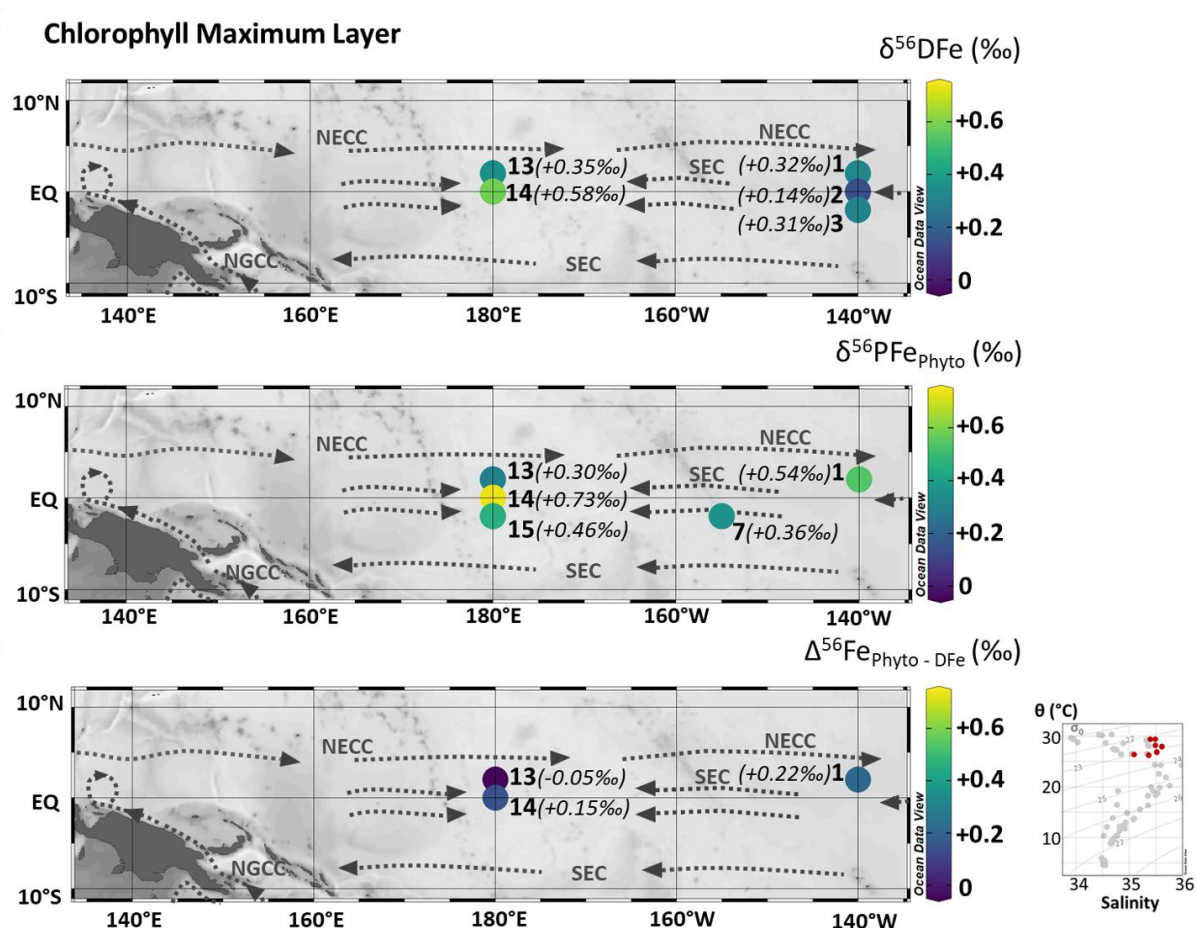
512 In the central equatorial Pacific region, the data are discussed within each of the five
 513 density layers defined in Section 2 in order to take into account the different water masses and

514 dominant currents. Western stations are included in the figures below solely to illustrate
 515 potential sources to this central Pacific area. To facilitate interpretation-comparison, the $\delta^{56}\text{Fe}$
 516 color coding-scales are different for each is the same-for-all density layers.

517

518 5.2.1. Surface layer, the chlorophyll maximum layer (< 120 m; < 23.8 kg.m⁻³)

519



520

521 Figure 8. From the top to bottom, samples collected in the chlorophyll maximum layer, maps
 522 of $\delta^{56}\text{DFe}$ (‰), $\delta^{56}\text{PFe}_{\text{Phyto}}$ (‰), and the difference between $\delta^{56}\text{PFe}_{\text{Phyto}}$ and $\delta^{56}\text{DFe}$. Station
 523 numbers are displayed next to the colored dots on the map. Main currents are represented: South
 524 Equatorial Current (SEC), North Equatorial CounterCurrent (NECC) and New Guinea Coastal
 525 Current (NGCC). In the bottom right corner, potential temperature (θ , °C) and salinity (S) of
 526 EUCFe samples. Samples in this chlorophyll maximum layer are shown in red. Values are
 527 shown in parentheses due to the large range, which limits color scale readability. Their
 528 measurement uncertainties can be found in Section 5.2.1 and Table 2.

529 Having both dissolved and particulate iron data in the open ocean surface layer,
 530 far from continental inputs, provides an opportunity to quantify isotopic fractionation
 531 associated with biological uptake, i.e., consumption of dissolved Fe by phytoplankton and its
 532 consequent transfer to the particulate pool. We focus on the chlorophyll maximum layer (found
 533 between 10 and 100 m, based on fluorescence data shown in Figure A2), also called the deep
 534 chlorophyll maximum (DCM), where the phytoplanktonic contribution to sampled particles is
 535 likely to be large. During the EUCFe cruise, the phytoplankton community was studied at
 536 station 2 at a depth of 10 meters (Marchetti et al., 2010), and in the chlorophyll maximum layer

537 at station 2, station 25, and at two other stations lacking iron isotope measurements (0°, 165°E
 538 and 0°, 170°W) (Johnson et al., 2010). The cyanobacteria *Prochlorococcus* and *Synechococcus*
 539 dominate this community, followed by small pennate diatoms such as *C. closterium* and *N.*
 540 *bicapitata* (Johnson et al., 2010; Marchetti et al., 2010). This observation is consistent with
 541 previous studies in this equatorial upwelling region, which report a predominantly
 542 cyanobacteria-based community (Chavez et al., 1990; Landry et al., 1996). Unicellular
 543 diazotrophic cyanobacteria were also identified throughout the cruise, primarily
 544 picocyanobacteria, while the larger *Trichodesmium* was found only in coastal waters (Bonnet
 545 et al., 2009).

546 PFe can be composed of lithogenic, biogenic, and chemogenic fractions. Chemogenic
 547 particles are formed by chemical reactions such as Fe oxyhydroxide precipitations and are
 548 frequently referred to as 'authigenic'. However, this term lacks precision as it merely designates
 549 material formed in situ, which could theoretically include biogenic fractions. ~~Particulate iron~~
 550 ~~(PFe) can originate from both authigenic or allogenic sources. In the chlorophyll maximum~~
 551 ~~layer, we assume that contains both authigenic and allogenic iron. We consider allogenic iron~~
 552 ~~to be entirely lithogenic, the predominant source of Fe in the equatorial Pacific.~~ Assuming
 553 Aluminum (Al) is entirely lithogenic (Murray et al., 1993; Frank et al., 1995; McManus et al.,
 554 1999; Cardinal et al., 2001; Dammshäuser, 2012), the lithogenic fraction of the particulate iron,
 555 [PFe]_{lithogenic}, is estimated by:

$$556 \quad [\text{PFe}]_{\text{lithogenic}} = [\text{PAI}]_{\text{measured}} \times \left(\frac{[\text{PFe}]}{[\text{PAI}]} \right)_{\text{reference material}} \quad (\text{Equation 3})$$

557 where [PAI]_{measured} is the measured particulate Al concentration and [PFe]/[PAI]_{reference material} is
 558 the ratio in a reference lithogenic material. Surface currents in our studied area are mainly
 559 eastward in the western Pacific and westward in the central Pacific. We therefore looked for
 560 reference lithogenic material on both the western and eastern boundaries of the Pacific basin.
 561 The Fe/Al ratios of igneous rocks from ~~the~~ Papua New Guinea (Tiangang et al., 2024) and of
 562 igneous rocks from the Galapagos Islands and the southwestern Andes basins of Peru (Wilson
 563 et al., 2022; Ccancapa-Cartagena et al., 2023) are equal to 0.502 mol.mol⁻¹ and 0.499 mol.mol⁻¹
 564 ¹ respectively. Given the ~~similarity~~ closeness of these ratios, we utilized an average value of
 565 0.50 mol.mol⁻¹ for all samples.

566 In the chlorophyll maximum layer, we found ~~that~~ an average of 42 % mol.mol⁻¹ of particulate
 567 iron (PFe) is lithogenic (Table A43). ~~with~~ The remaining 58 % mol.mol⁻¹ can be attributed to
 568 ~~bioauthigenic and chemogenic sources.~~ The chemogenic fraction cannot be distinguished and
 569 quantified in the present study (this would have required, for example, direct measurements of
 570 phytoplankton stoichiometry and phosphorus), and there is no known isotopic signature specific
 571 to this chemogenic fraction in the literature (which is essential for Equation 4). Because we are
 572 looking at samples taken in the chlorophyll maximum, we will assume in the following that
 573 ~~Assuming that, in the chlorophyll maximum away from lithogenic inputs of Fe, authigenic Fe~~
 574 ~~consists entirely of the chemogenic Fe is negligible.~~ This assumption is supported by
 575 observations reporting minimum chemogenic contribution in the chlorophyll maximum layer
 576 (Sofen et al., 2013) and modelling work estimating that the biogenic fraction dominates in the
 577 central equatorial Pacific (Tagliabue et al., 2023). We also assume that biogenic ~~organic~~ Fe is
 578 entirely ~~and furthermore~~ of phytoplanktonic Fe (PFe_{authigenic} = PFe_{Phyto}) and assuming mass
 579 conservation, δ⁵⁶PFe_{Phyto} can be estimated from:

$$580 \quad [\text{PFe}]_{\text{Phyto}} \cdot \delta^{56}\text{PFe}_{\text{Phyto}} \approx [\text{PFe}] \cdot \delta^{56}\text{PFe} - [\text{PFe}]_{\text{lithogenic}} \cdot \delta^{56}\text{PFe}_{\text{lithogenic}} \quad (\text{Equation 4})$$

581 where [PFe] and δ⁵⁶PFe are the measured particulate Fe concentration and isotopic composition.
 582 The lithogenic PFe is assumed to be characterized by average crustal signature δ⁵⁶PFe_{lithogenic} =
 583 +0.07 ± 0.02 ‰ (Poitrasson, 2006). The estimated isotope compositions of phytoplanktonic
 584 PFe are shown in Figure 8 and Table A43. δ⁵⁶PFe_{Phyto} varies from +0.30 ± 0.12 ‰ to

585 +0.73 ± 0.17 ‰. Propagation of uncertainties for Fe and Al concentrations and Fe isotopes in
586 both the samples and the reference material implies uncertainties for $\delta^{56}\text{PFe}_{\text{Phyto}}$ significantly
587 higher than those of our initial data.

588 At three stations, the isotope data are available for both the dissolved and the
589 phytoplanktonic iron. This allows an estimate of isotope fractionation associated with
590 phytoplankton uptake. Assuming two simple isotopic models, either an equilibrium
591 fractionation model (implying bidirectional chemical reactions) or a kinetic fractionation model
592 in which phytoplankton is the instantaneous product of DFe (implying unidirectional chemical
593 reactions), the isotopic fractionation can be calculated, with the same simple equation (Hayes,
594 2004):

$$595 \Delta^{56}\text{Fe}_{\text{Phyto-DFe}} = \delta^{56} \text{PFe}_{\text{Phyto}} - \delta^{56}\text{DFe} \quad (\text{Equation 5})$$

596 This leads to $\Delta^{56}\text{Fe}_{\text{Phyto-DFe}} = +0.22 \pm 0.21 \text{ ‰}$ at station 1, $-0.05 \pm 0.14 \text{ ‰}$ at station 13 and
597 $+0.15 \pm 0.19 \text{ ‰}$ at station 14, with a grand average value of $\Delta^{56}\text{Fe}_{\text{Phyto-DFe}} = +0.11 \pm 0.28 \text{ ‰}$
598 (2SD, n=3) (Figures 8 and Table A43). Given the uncertainties, we cannot conclude that there
599 is isotopic fractionation associated with biological uptake, but our data indicate that if it exists,
600 it is small and lies between -0.17 and +0.39 ‰ ($+0.11 \pm 0.28$) at a 95% confidence level.

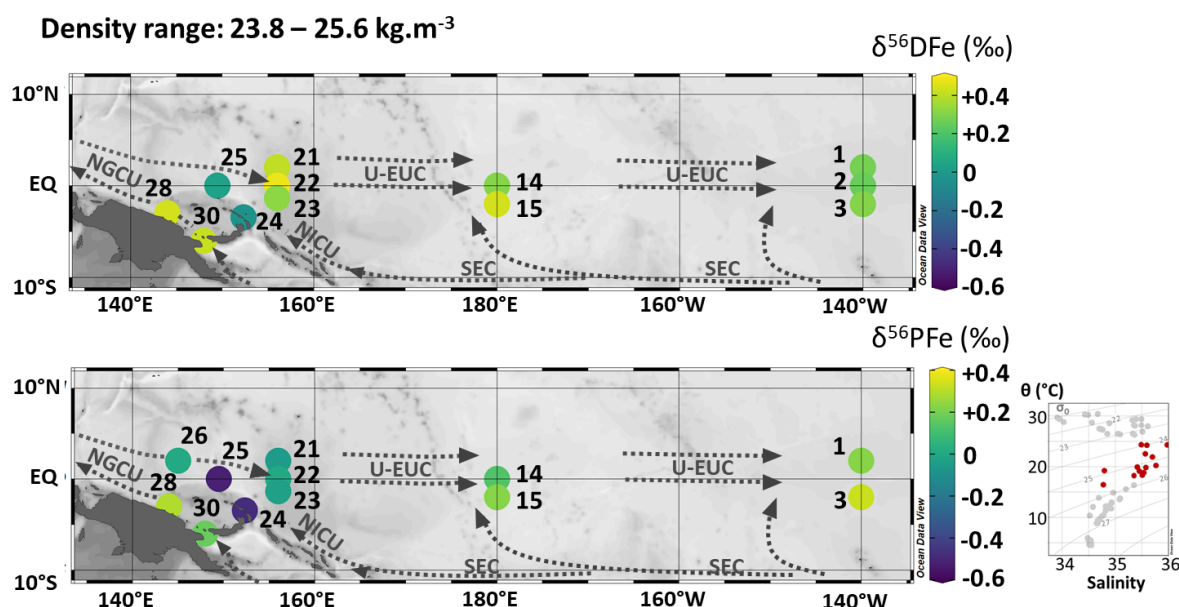
601 These results can be compared with previous studies. Some suggest preferential uptake
602 of light and others of heavy isotopes. From the same cruise, Radic et al. (2011) found
603 $\Delta^{56}\text{Fe}_{\text{Phyto-DFe}} = -0.25 \pm 0.10 \text{ ‰}$ (2SD) with one model and $-0.13 \pm 0.11 \text{ ‰}$ (2SD) with a second
604 model. While the first model was based solely on DFe data, the second incorporated PFe data
605 assuming PFe was exclusively phytoplanktonic, whereas our results indicate a substantial
606 lithogenic contribution at the open ocean stations (Table A43). [Additional data and novel
607 methodological approaches have refined these estimates.](#) Off New Zealand, during the annual
608 spring bloom, Ellwood et al. (2015) estimated an isotopic fractionation of -0.54 ‰. In [that study
609 this work](#) the isotopic signatures of the particles were used, but not corrected for their lithogenic
610 fractions, despite proximity to the mainland, and fractionation uncertainties were not discussed.
611 In two Antarctic coastal polynyas, preferential uptake of light isotopes [washave been](#) suggested
612 based on water mass DFe signatures alone (without PFe data), with isotopic fractionation of -1
613 ‰ ($\alpha = \delta^{56}\text{Fe}_{\text{Biomass}} / \delta^{56}\text{Fe}_{\text{Seawater}} = 0.999$) (Sieber et al., 2021) and of -1.8 to -1 ‰ ($\alpha = 0.9982$
614 to 0.9990) (Tian et al., 2023). However, both studies highlighted the co-occurrence of multiple
615 mechanisms and, therefore, of several isotopic fractionation processes in the surface layer.
616 Ellwood et al. (2020) conducted a study using both DFe and PFe isotope data in a 1-D model,
617 and found isotopic fractionation values for biological uptake ranging from -1 ‰ (in a simplified
618 model considering only biological uptake) to -0.6 ‰ when using a more sophisticated model
619 representing additional processes (regeneration, scavenging and complexation) in a cold-core
620 eddy in the Southern Ocean. Again, fractionation uncertainties were not discussed in these three
621 studies. Finally, in the North Atlantic, two studies suggested a positive fractionation
622 (contrasting with the previous studies) based on water mass DFe signatures (no PFe data) and
623 without quantification (Conway and John, 2014; Klar et al., 2018). [Culture experiments
624 examining isotopic fractionation by several diatom and a coccolithophore species \(not the
625 dominant species in our samples \(Johnson et al., 2010; Marchetti et al., 2010\)\) revealed ‘no
626 clear relationship to species, growth rate, or Fe concentration’ for biological uptake, possibly
627 due to the sensitivity of kinetic isotope effects \(John et al., 2024\). During these experiments,
628 biological uptake induced smaller fractionation \(-1.3 ‰ to +0.60 ‰, mean \$+0.20 \pm\$
629 \$0.38 \text{ ‰}\$, 1SD, n=62\) compared to abiotic processes \(approximately -4 ‰ to +5 ‰\). These
630 laboratory observations align with our in situ observations, although a comparison is not
631 straightforward because iron acquisition processes are very different in cyanobacteria \(Sutak et
632 al., 2020\). These authors suggested that seawater \$\delta^{56}\text{Fe}\$ may not be greatly impacted by
633 biological uptake \(John et al., 2024\); a conclusion consistent with the findings of Lacan et al.,
634 2008 and Radic et al., 2011.](#)

635 The differences in biological fractionation probably reflect variations in phytoplankton
 636 community composition, ligand types (John et al., 2024), regional variability, and
 637 methodological approaches ~~regional variabilities, including differences in phytoplankton~~
 638 ~~community, as well as differences in methodology~~ such as the direct measurement of particles
 639 and the consideration of their phases. Potential iron fractionation during biological uptake, if it
 640 occurs, may depend on numerous parameters, including species-specific iron acquisition
 641 processes (Sutak et al., 2020), as well as pH, ligand, and reductant types, which strongly
 642 influence kinetic isotope effects (John et al., 2024). Our study region is particularly challenging
 643 in this regard, as it is a cyanobacteria-dominated system where isotopic fractionation processes
 644 remain poorly understood (Mulholland et al., 2015; Swanner et al., 2017). Iron isotope
 645 fractionation by diazotrophic cyanobacteria has not been investigated, despite these organisms
 646 contributing disproportionately to Fe uptake relative to their numerical abundance (Lory et al.,
 647 2022). The present analysis does not allow us to draw conclusions regarding a preferential
 648 uptake of heavy or light iron isotopes during biological uptake. However, our results confirm
 649 that this fractionation is small, likely not larger than a few tenths of a per mil. They align with
 650 a ~~previous former~~ study, in the Southern Ocean, where fractionation ~~had was quantified with~~
 651 a small amplitude, $|\Delta^{56}\text{Fe}_{\text{Phyto-DFe}}| < 0.32 \text{ ‰}$, with no conclusion about the direction (Lacan et al.,
 652 2008), and culture experiments (John et al., 2024). Our analysis emphasizes the importance of
 653 taking into account error propagations and lithogenic contributions to the particulate phases,
 654 ~~even~~ in the chlorophyll maximum in the open ocean.

655

656 5.2.2. Subsurface layer (110 – 220 m; 23.8 – 25.6 kg.m⁻³), upper EUC

657



658

659 Figure 9. Map of dissolved ($\delta^{56}\text{DFe}$) and particulate ($\delta^{56}\text{PFe}$) iron isotopes for samples with
 660 potential densities between 23.8 and 25.6 kg.m⁻³. Station numbers are displayed next to the
 661 colored dots. Main currents are represented: the upper Equatorial Undercurrent (U-EUC), the
 662 South Equatorial Current (SEC), the New Guinea Coastal Undercurrent (NGCU) and the New
 663 Ireland Coastal Undercurrent (NICU). In the bottom right corner, potential temperature (θ , °C)
 664 and salinity (S) of EUCFe samples. Samples in this density layer are shown in red.

665 The subsurface layer is composed of three water masses: the South Pacific Tropical
 666 Water (SPTW) (stations 3 and 15), the South Pacific Equatorial Water (SPEW) (stations 2, 14,

667 21, 22, 23, 24, 25, 28 and 30) and the North Pacific Equatorial Water (NPEW) (stations 1 and
 668 26) (Figure 9). At the equator, seawater within SPEW is subject to substantial renewal as it
 669 flows eastward from the western Pacific (140°E) to the central equatorial Pacific (140°W)
 670 (Tsuchiya et al., 1989; Grenier et al., 2011). This renewal is largely driven by equatorial
 671 upwelling which creates divergence in subsurface waters and subsequently generates
 672 meridional currents from both the northern and southern subtropical gyres toward the equator.
 673 These gyres ventilate the upper Equatorial Undercurrent (U-EUC), contributing approximately
 674 9 Sv of the total 28 Sv contribution at 140°W, thus accounting for nearly one third of the upper
 675 EUC flow (Grenier et al., 2011).

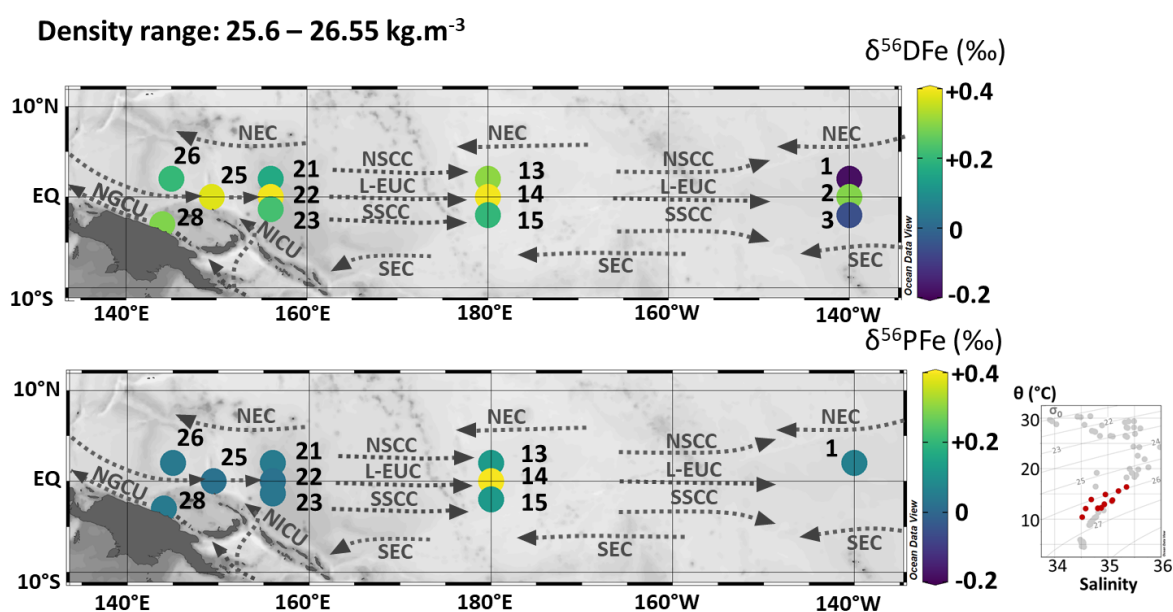
676 We observed that $\delta^{56}\text{DFe}$ values were equal within uncertainties along the meridional
 677 transects between 2°N and 2°S (+0.40 ‰, +0.37 ‰ and +0.28 ‰ at 156°E, 180°E and 140°W,
 678 respectively) and similar consistency is observed for $\delta^{56}\text{PFe}$ (-0.03 ‰, +0.18 ‰ and +0.28 ‰
 679 at the three same sections, Figure 9 and Table 2). This isotopic homogeneity is consistent with
 680 the prevailing ocean circulation in the subsurface layer. Zonally, a slight decrease of $\delta^{56}\text{DFe}$
 681 values and a slight increase of $\delta^{56}\text{PFe}$ values were observed eastward.

682 A comparison of DFe isotopic compositions ($\delta^{56}\text{DFe}$) in EUCFe samples with data from
 683 the subtropical gyres provides further insight. While no data are available for the north
 684 subtropical gyre, this density layer has been documented in the south subtropical gyre along
 685 170°W (GP19 cruise) at 10°S (Station 19) with $\delta^{56}\text{DFe} = +0.64 \pm 0.32$ ‰, and at the equator
 686 (Station 21) with $\delta^{56}\text{DFe} = +0.70 \pm 0.35$ ‰ (GEOTRACES Intermediate Data Product Group,
 687 2023). These two datapoints are in good agreement with each other. They may appear to
 688 be could seem significantly different from our data ($\sim -0.37 \pm 0.1$ ‰ at 180°E), however given
 689 their uncertainties, they are in reasonable agreement. They do not help explain the slight
 690 eastward decrease of the $\delta^{56}\text{DFe}$ along the equator described above.

691 Overall, despite small variations, these observations suggest a relatively wide isotopic
 692 homogeneity at subsurface depths (110 – 220 m) likely driven by equatorial upwelling and the
 693 subsequent meridional transport of seawater.

694

695 5.2.3. Lower part of EUC: Central Waters (170 – 320 m; 25.6 – 26.55 kg.m⁻³)



696

697 Figure 10. Map of dissolved ($\delta^{56}\text{DFe}$) and particulate ($\delta^{56}\text{PFe}$) iron isotopes for samples
698 with potential densities between 25.6 and 26.55 kg.m^{-3} . Station numbers are displayed next to
699 the colored dots. Main currents are represented: the lower Equatorial Undercurrent (L-EUC),
700 the North and South Subsurface Countercurrents (NSCC and SSCC), [the North and South](#)
701 [Equatorial Current \(NEC and SEC\)](#), the New Guinea Coastal Undercurrent (NGCU) and the
702 New Ireland Coastal Undercurrent (NICU). In the bottom right corner, potential temperature
703 (θ , $^{\circ}\text{C}$) and salinity (S) of EUCFe samples. Samples in this density layer are shown in red.

704

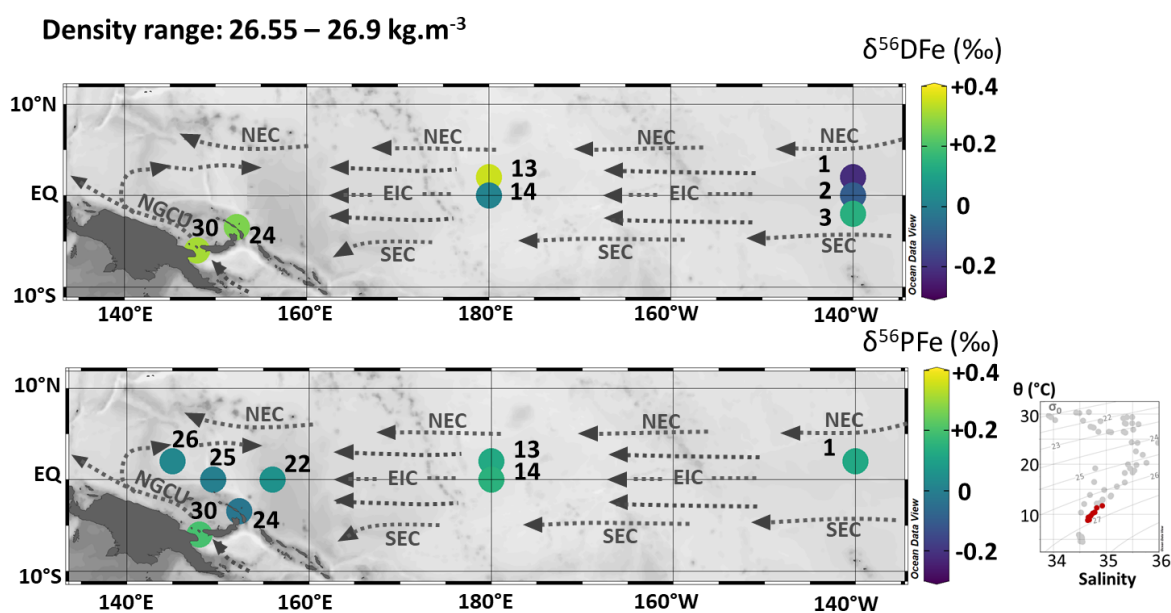
705 The density layer between 25.6 and 26.55 kg.m^{-3} is composed of two water masses: the
706 Western South Pacific Central Water (WSPCW) (stations 1, 2, 3, 14, 15, 22, 23, 25, 28) and the
707 North Pacific Central Water (NPCW) (stations 13, 21, 26) ([Figure 2](#)). WSPCW is characterized
708 by [the](#) salinity maximum of central waters while NPCW represents [the](#) salinity minimum.
709 The lower part of the EUC (L-EUC) is located in this density layer ([Figure 10](#)). This current is
710 of particular importance, since it is the major vector for [the](#) Fe transport along the equator from
711 the western to the eastern Pacific. The lower EUC is not significantly influenced by the
712 equatorial upwelling in the western equatorial Pacific, and water mostly originates from the
713 PNG region (Grenier et al., 2011).

714 Along the equator, at stations 25, 22, 14 and 2, samples have similar DFe isotopic
715 composition (around +0.36 ‰), highlighting the lack of significant additional Fe sources [to](#)
716 the lower EUC (Tsuchiya et al., 1989; Radic et al., 2011). $\delta^{56}\text{DFe}$ values are equal within
717 uncertainties ([Figure 10](#) and [Table 2](#)). This suggests that the $\delta^{56}\text{DFe}$ signature is maintained
718 over long distances within the EUC, a pattern previously reported by Radic et al. (2011) at two
719 stations, and here confirmed as far east as 140°W . In contrast, $\delta^{56}\text{PFe}$ cannot be evaluated at
720 station 2 due to missing PFe data, and values from stations 22 and 14 displayed significantly
721 different values. These findings confirm the central role of the EUC [for](#) DFe transport across
722 the Pacific. While earlier studies based on Fe concentrations suggested such transport (Slemons
723 et al., 2012), isotopic data now confirm this conclusion and the fact that dissolved iron isotopic
724 signature may be preserved, in [certain circumstances](#) over more than 7 800 km (from station 25
725 to station 2). Long distance preservation of $\delta^{56}\text{DFe}$ signature has been underlined before for
726 deeper layers, notably in the North Pacific and eastern Pacific with Fe transport from
727 sedimentary and hydrothermal sources (Fitzsimmons et al., 2017; John et al., 2018; Sieber et
728 al., 2024). [Such a long distance of preservation of the \$\delta^{56}\text{DFe}\$ signature had never been observed](#)
729 [before](#).

730 Samples from stations 1 and 3 differ significantly from the other samples. They are
731 characterized by negative dissolved iron isotopic compositions (-0.19 and -0.06 ‰) ([Figure 10](#)
732 and [Table 2](#)). They are characterized by oxygen concentrations which are notably lower than
733 those typically found in the core of the EUC (43 and 25 $\mu\text{mol.kg}^{-1}$, compared to typical values
734 around 130 $\mu\text{mol.kg}^{-1}$). The currents supplying these stations, [the](#) SEC and NEC, originate
735 from the east. These three observations support the conclusion that their Fe content [may](#)
736 [originate](#), at least partially, from the Californian and/or Peruvian oxygen minimum zones
737 (OMZ). Those have been documented before, with negative or zero $\delta^{56}\text{DFe}$ values in the
738 Californian OMZ (John et al., 2012), and DFe concentrations and isotopic compositions, around
739 1 nM and -0.5 ‰, observed around 12°S near the Peruvian coast (85 to 80°W) during the GP16
740 cruise (John et al., 2018). As above, this suggests a $\delta^{56}\text{DFe}$ signature preservation over long
741 distances, [one](#) the order of 6,400 km.

742 In [the](#) density layer, [that](#) of the lower EUC, iron isotopes reveal the presence of two
743 distinct Fe sources in the central Pacific, lithogenic inputs from Papua New Guinea transported
744 within the EUC, and also [a](#) [likely](#) additional eastern source from the eastern Pacific oxygen
745 minimum zones.

746 **5.2.4. South Antarctic Mode Water and Lower Central Waters (340 – 480 m; 26.55 –**
 747 **26.9 kg.m⁻³)**



748
 749 Figure 11. Map of dissolved ($\delta^{56}\text{DFe}$) and particulate ($\delta^{56}\text{PFe}$) iron isotopes for samples with
 750 potential densities between 26.55 and 26.9 kg.m⁻³. Station numbers are displayed next to the
 751 colored dots. Main currents are represented: the Equatorial Intermediate Current (EIC), the
 752 North and South Equatorial Current (NEC and SEC), and the New Guinea Coastal Undercurrent
 753 (NGCU). In the bottom right corner, potential temperature (θ , °C) and salinity (S) of EUCFe
 754 samples. Samples in this density layer are shown in red.

755 The density layer between 26.55 and 26.9 kg.m⁻³ is composed of two water masses: the
 756 South Antarctic Mode Water (SAMW) (stations 22, 24, 25) and the Western South Pacific
 757 Central Water (WSPCW) (stations 1, 2, 3, 13, 14, 26, 30). In contrast to the shallower density
 758 layers, where currents predominantly flow eastward, this deeper layer exhibits westward
 759 currents (Figure 11).

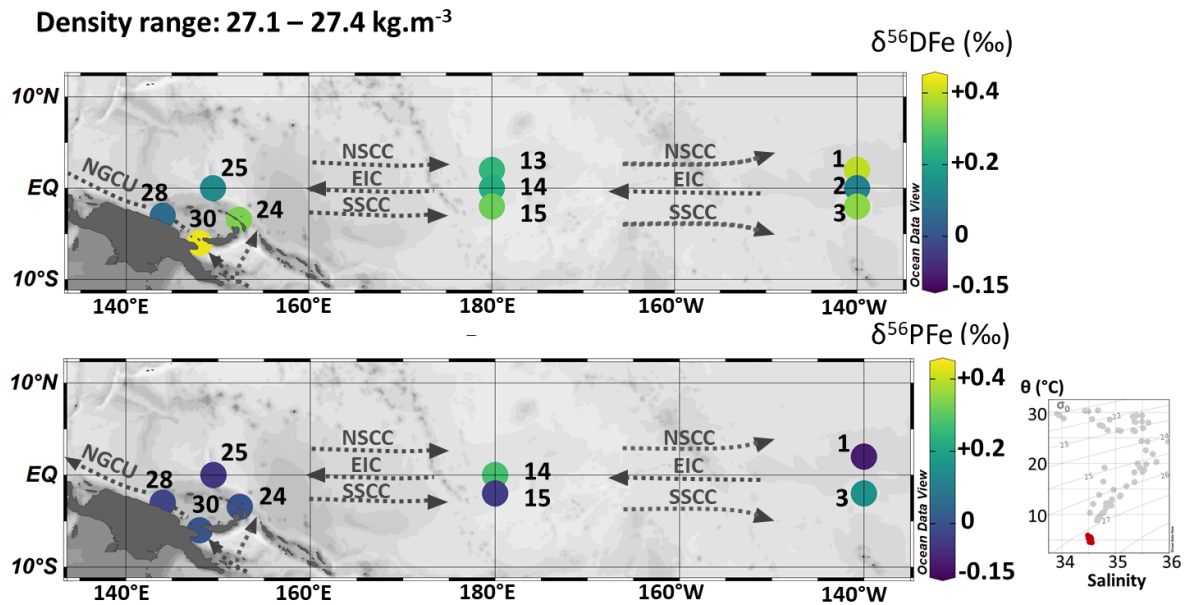
760 DFe isotopic compositions at stations 1, 2, 3, 13 and 14 were variable: negative or near
 761 zero $\delta^{56}\text{DFe}$ at stations 1, 2 and 14 (between -0.22 and +0.01 ‰) and positive $\delta^{56}\text{DFe}$ at stations
 762 3 and 13 (+0.14 and +0.35 ‰) (Figure 11 and Table 2). $\delta^{56}\text{DFe}$ values increased westward from
 763 station 1 (-0.22 ± 0.09 ‰) to station 13 (+0.35 ± 0.07 ‰) and from station 2 (-0.10 ± 0.07 ‰)
 764 to station 14 (+0.01 ± 0.07 ‰). This westward increase in $\delta^{56}\text{DFe}$ follows the predominant
 765 direction of zonal currents. It is consistent with data from GP19 at 170°W at the equatorial
 766 station 21 (-0.07 ± 0.05 ‰, depth of 469 m) (GEOTRACES Intermediate Data Product Group,
 767 2023). In contrast, $\delta^{56}\text{PFe}$ values at stations 1, 13, and 14 were indistinguishable from one
 768 another and similar to the UCC reference value. Samples from stations 1, 2, 3, 13 and 14
 769 exhibited low oxygen concentrations (< 64 $\mu\text{mol.kg}^{-1}$). In contrast, ~~to~~ samples from the western
 770 equatorial Pacific (stations 22, 24, 25, 26 and 30) ~~had where~~ oxygen concentrations ranging
 771 from 101 to 162 $\mu\text{mol.kg}^{-1}$.

772 These isotopic and oxygen observations suggest an Fe source from the eastern Pacific
 773 oxygen minimum zones (OMZ) and a progressive decline in the influence of eastern Pacific
 774 waters with the increase of $\delta^{56}\text{DFe}$ westward. It is consistent with our understanding of large-
 775 scale circulation patterns at these depths across the Pacific basin, and with the signatures of
 776 these areas as described above (John et al., 2012, 2018). In contrast, particulate data were

777 indistinguishable from those of the UCC all along the EUCFe cruise and therefore do not reflect
778 hydrodynamic structures.

779

780 5.2.5. Intermediate Waters (SeqIW and AAIW) (720 – 1 000 m; 27.1 – 27.4 kg.m⁻³)



781

782 Figure 12. Map of dissolved ($\delta^{56}\text{DFe}$) and particulate ($\delta^{56}\text{PFe}$) iron isotopes for samples with
783 potential densities between 27.1 and 27.4 kg.m⁻³. Station numbers are displayed next to the
784 colored dots. Main currents are represented: the Equatorial Intermediate Current (EIC), the
785 North and South Subsurface Countercurrents (NSCC and SSCC), and the New Guinea Coastal
786 Undercurrent (NGCU). In the bottom right corner, potential temperature (θ , °C) and salinity (S)
787 of EUCFe samples. Samples in this density layer are shown in red.

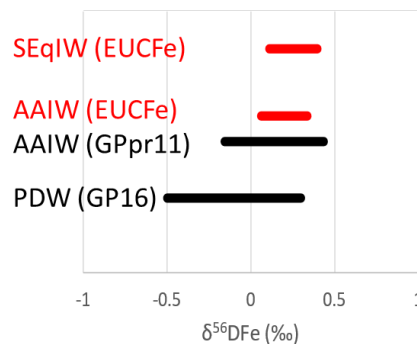
788 The density layer between 27.1 and 27.4 kg.m⁻³ is composed of two intermediate water
789 masses: the South Equatorial Intermediate Water (SeqIW) (stations 1, 2, 3, 13, 14, 15, 25) and
790 the Antarctic Intermediate Water (AAIW) (stations 24, 28, 30) (Figure 12). In this layer, the
791 Equatorial Intermediate Current (EIC), a westward current, is surrounded by two eastward
792 currents, the North and South Subsurface Countercurrents (NSCC and SSCC). The water of the
793 EIC is sheared between the NSCC and SSCC currents at about 2°N and 2°S, causing mixing of
794 water brought in by different currents.

795 Along the equator, a uniform $\delta^{56}\text{DFe}$ signature was observed between stations 2, 14 and
796 25, around +0.15 ‰. North and south of it, in the NSCC and the SSCC, the $\delta^{56}\text{DFe}$ signatures
797 were significantly heavier, around +0.32 ‰ and +0.34 ‰ respectively, and did not vary
798 significantly zonally. This is consistent with the hydrodynamic structure (westward flowing
799 EIC at the Equator and eastward flowing NSCC and SSCC at 2°N and 2°S) and may also reflect
800 slightly lighter signatures originating from the eastern Pacific compared to the western Pacific.
801 In contrast, no such consistency was observed for the $\delta^{56}\text{PFe}$ values.

802 [Figure 13 compares](#) $\delta^{56}\text{DFe}$ of the AAIW and SeqIW from this study [are compared](#) with
803 data from the South Pacific, GPpr11 (in the Southern Ocean, south of Australia) and GP16
804 cruises (John et al., 2018; Ellwood et al., 2020) [in Figure 13](#). The EUCFe AAIW signature
805 (sampled at the western stations 24, 28 and 30 only) fell within the range of [datathose](#)-previously
806 reported, but [with lessdisplayed a smaller](#) variability (from +0.06 to +0.44 ‰, with an average
807 of +0.28 ‰). As explained previously this likely reflects the impact of [particulate - dissolved](#)

808 [particle/dissolved](#) reversible exchange and non-reductive dissolution processes which buffer
809 the isotopic signature of this water mass toward about +0.3 ‰, in the PNG area.

810 The SEqIW (sampled at stations 1, 2, 3, 13, 14, 15, and 25) results from the mixing
811 between the AAIW and the Pacific Deep Water (PDW). Its signatures fall within the range
812 observed for those waters masses in previous studies, but \rightarrow they fall in the heavy [range](#) of
813 those [values](#) and \rightarrow again have a smaller variability (from +0.11 to +0.40‰, average
814 value of +0.24‰). This confirms 1) the large contribution of AAIW to the iron content of
815 SEqIW and the fact that AAIW transits from the South through the PNG area and notably Vitiaz
816 Strait before spreading in the equatorial band (Tomczak and Godfrey, 2003; Bostock et al.,
817 2010), and 2) that the PDW contributing to the SEqIW reaches the Equatorial band with minor
818 contribution from eastern Pacific OMZ derived iron, characterized by light isotopic signatures
819 (John et al 2018).



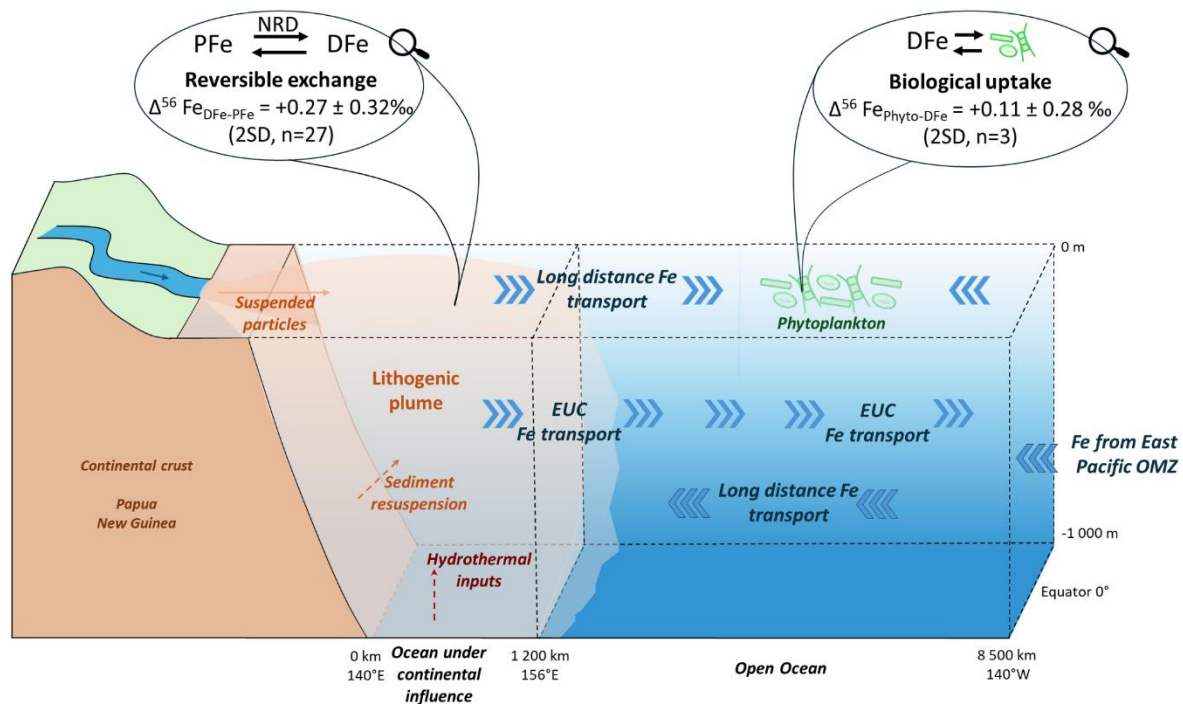
820

821 Figure 13. Comparison of $\delta^{56}\text{DFe}$ values in different water masses: the SEqIW sampled during
822 EUCFe cruise (this study), the AAIW sampled during EUCFe (this study) and GPpr11 cruises
823 (Ellwood et al., 2020) and the PDW sampled during GP16 cruise (John et al., 2018).

824

825 6. CONCLUSIONS

826 [Figure 14 shows](#) The main conclusions resulting from [this](#) study of [the](#) concentrations
827 and isotope compositions for iron in the upper 1 000 meters of the water column between 140°E
828 and 140°W [are shown in Figure 14.](#)



829

830 Figure 14. Illustration of Fe transport and transformation along the EUCFe cruise along the equator from the surface to 1 000 meters depth. OMZ stands for oxygen minimum zone.
831

832 The goal of the EUCFe cruise was to determine the distribution of Fe along the equator
833 between Papua New Guinea (PNG) and 140°W and to investigate the role of the Equatorial
834 Undercurrent (EUC) in the Fe supply to the central equatorial Pacific. This study reports
835 seawater Fe concentrations and isotopic compositions ($\delta^{56}\text{Fe}$) in both the dissolved (DFe) and
836 particulate (PFe) phases. By adding data from 11 additional stations, this work significantly
837 enriches the data previously published ~~from~~ four stations ~~on~~ from the same cruise (Radic et
838 al., 2011; Labatut et al., 2014) and introduces a novel suggestion about an iron source from the
839 eastern Pacific OMZ. The isotopic compositions ranged from -0.25 to +0.79 ‰ for dissolved
840 iron and from -0.56 to +0.48 ‰ for particulate iron. Two distinct groups of stations were
841 identified on the basis of Fe concentrations: western Pacific stations displaying PFe and DFe
842 concentrations approximately seven times and twice larger than typical open ocean
843 concentrations, respectively (stations 21, 22, 23, 24, 25, 26, 28, and 30, all located ~~east~~ within
844 1 200 km of the Papua New Guinea coast) and central Pacific open ocean stations, with PFe
845 and DFe typical of the open ocean (stations 1, 2, 3, 7, 13, 14, and 15).

846 In the western equatorial Pacific, a large predominance of PFe concentrations over that
847 of DFe was observed (80 % mol.mol^{-1} PFe compared to total Fe, on average). The isotope
848 signature of ~~PFe~~ these particles approached that of the ~~UCC~~ upper continental crust
849 confirmings the major influence of previously documented lithogenic inputs from PNG in this
850 area (Milliman et al., 1999; Slemons et al., 2012). At two stations, distinctly light $\delta^{56}\text{DFe}$ and
851 $\delta^{56}\text{PFe}$ signatures suggested local hydrothermal inputs. At all stations of this western area, a
852 systematic positive difference between $\delta^{56}\text{DFe}$ and $\delta^{56}\text{PFe}$ was observed, $\Delta^{56}\text{Fe}_{\text{DFe-PFe}} = +0.27$
853 ± 0.32 ‰ (2SD, n=27). This is interpreted as the result of equilibrium isotopic fractionation, ~~in~~
854 other words the co-occurrence of chemical fluxes from both phases toward the other. ~~resulting~~
855 from a permanent and reversible exchange between dissolved and particulate Fe phases. This
856 probably reflects processes similar to the reversible scavenging process proposed for Th or REE
857 (Bacon and Anderson, 1982; Nozaki et al., 1987; Nozaki and Alibo, 2003), as previously
858 proposed (Abadie et al., 2017). ~~Desorption and/or ligand-promoted dissolution are potential~~
859 mechanisms, though the exact processes involved remain unclear (Abadie et al., 2017; Homoky
860 et al., 2021). Isotopic signatures suggest that Fe is primarily released via non-reductive release

861 of dissolved Fe from suspended particles and/or oxic sediment. New data from 11 additional
862 stations demonstrate that this process extends up to 1 200 km from the Papua New Guinea coast.

863 In the open ocean, between 180°E and 140°W, data from the chlorophyll maximum
864 layer were used to estimate isotopic fractionation associated with phytoplankton uptake. Our
865 data suggest that isotopic fractionation during phytoplankton uptake is small, on the order of a
866 few tenths of per mil. Estimates of fractionation due to biological uptake must include
867 consideration of phytoplankton composition, dominated here by cyanobacteria. Just below this
868 layer, within the upper EUC, $\delta^{56}\text{Fe}$ values remain homogeneous across a broad region spanning
869 2°N to 2°S and 156°E to 140°W, consistent with equatorial upwelling and meridional Fe inputs.
870 In the lower EUC, a DFe isotopic signature of $\sim +0.36\text{‰}$, from ~~the~~ Papua New Guinea ~~area~~
871 ~~all the way~~ eastward ~~to~~ at least ~~to~~ 140°W, confirms the origin of the DFe carried within this
872 current toward the HNLCC~~L~~ area. However, an additional Fe source was identified bordering
873 the lower EUC at 2°N and 2°S likely originating from the oxygen minimum zones (OMZ) of
874 the eastern Pacific. This OMZ Fe source ~~appears to be~~ ~~is~~ also traced deeper within central waters
875 (200–500 m depth). The preservation of distinct Fe isotopic signatures over ~~unprecedented~~ long
876 distances, 7 800 km, is a key observation of this study. Finally, the limited variability of the
877 $\delta^{56}\text{DFe}$ signatures in intermediate waters, ~~averaging~~ ~~average of~~ $+0.24\text{‰}$, confirms the major
878 influence of AAIW transiting through the PNG area in the intermediate waters in the EUCFe
879 area.

880 In conclusion, this study demonstrates the substantial influence of lithogenic inputs
881 along ocean margins, where the water column (at least down to 1000 m) is affected by
882 ~~permanent and reversible exchange equilibrium fractionation~~ between dissolved and particulate
883 phases. It suggests the significance of non-reductive processes releasing dissolved iron from
884 particulate iron. This non-reductive dissolution (NRD), ~~occurs~~ ~~occurring~~ either at the
885 sediment/seawater interface (i.e., external sources), or within the water column (i.e., internal
886 processes). This highlights the need for a better understanding of these non-reductive DFe –
887 PFe interactions, through in situ explorations, experimental work and biogeochemical
888 modelling. Such processes likely influence the biogeochemical cycling of multiple elements.
889 This study ~~also~~ allowed identification of long-distance iron transport by ocean currents ~~from an~~
890 ~~ocean margin~~ and clarified the key role of the Equatorial Undercurrent (EUC). Finally, it
891 ~~suggested~~s minor fractionation associated to phytoplankton uptake.

892

894 **Table A1.** Sensitivity tests for different scenarios. Mean PFe concentration, Flux PFe_{SWout}, the
 895 required external sources flux, Flux PFe_{aerosol} and Flux PFe_{riverine} contribution to required
 896 external sources (% g.g⁻¹) according to different calculation methods. Go-Flo replicates are
 897 duplicate samples taken at sea, from the same cast.

	Go-Flo bottle replicates considered separately and with the highest value (29.45 nmol.kg ⁻¹)	Go-Flo bottle replicates considered separately and without the highest value (29.45 nmol.kg ⁻¹)	Go-Flo bottle replicates averaged and with the highest value (29.45 nmol.kg ⁻¹)	Go-Flo bottle replicates averaged and without the highest value (29.45 nmol.kg ⁻¹)
Mean PFe concentration (nmol.kg ⁻¹)	3.6 ± 4.8 (1SD)	2.9 ± 2.3 (1SD)	3.8 ± 5.0 (1SD)	3.0 ± 2.5 (1SD)
Flux PFe _{SWout} (10 ⁶ g.day ⁻¹)	337.9	272.2	356.7	281.6
Required external sources flux: Flux PFe _{SWout} - Flux PFe _{SWin} (10 ⁶ g.day ⁻¹)	323.5	257.8	342.2	267.1
Aerosol PFe flux contribution to required external sources (% g.g ⁻¹)	82.9	104.0	78.3	100.3
Riverine PFe flux contribution to required external sources (% g.g ⁻¹)	37,099.0	46,556.2	35,064.0	44,920.3

898

899 **Table A2.** Daily precipitation rates (mm.day⁻¹) over the entire region considered in the box
 900 model (133°E–177°W, 9°S–15°N) from September 20 to 30, 2006. The data was obtained from
 901 Nasa Giovanni data product TRMM (3B42 Daily v7)
 902 (<https://giovanni.gsfc.nasa.gov/giovanni/>).

Date	Precipitation Rate (TRMM 3B42 Daily v7) access in December 2025 from Nasa Giovanni data product TRMM (mm.day ⁻¹)
September 20, 2006	7.5
September 21, 2006	7.7
September 22, 2006	10.6
September 23, 2006	8.3
September 24, 2006	10.2
September 25, 2006	9.0
September 26, 2006	11.4
September 27, 2006	13.9

September 28, 2006

14.4

September 29, 2006

16.5

September 30, 2006

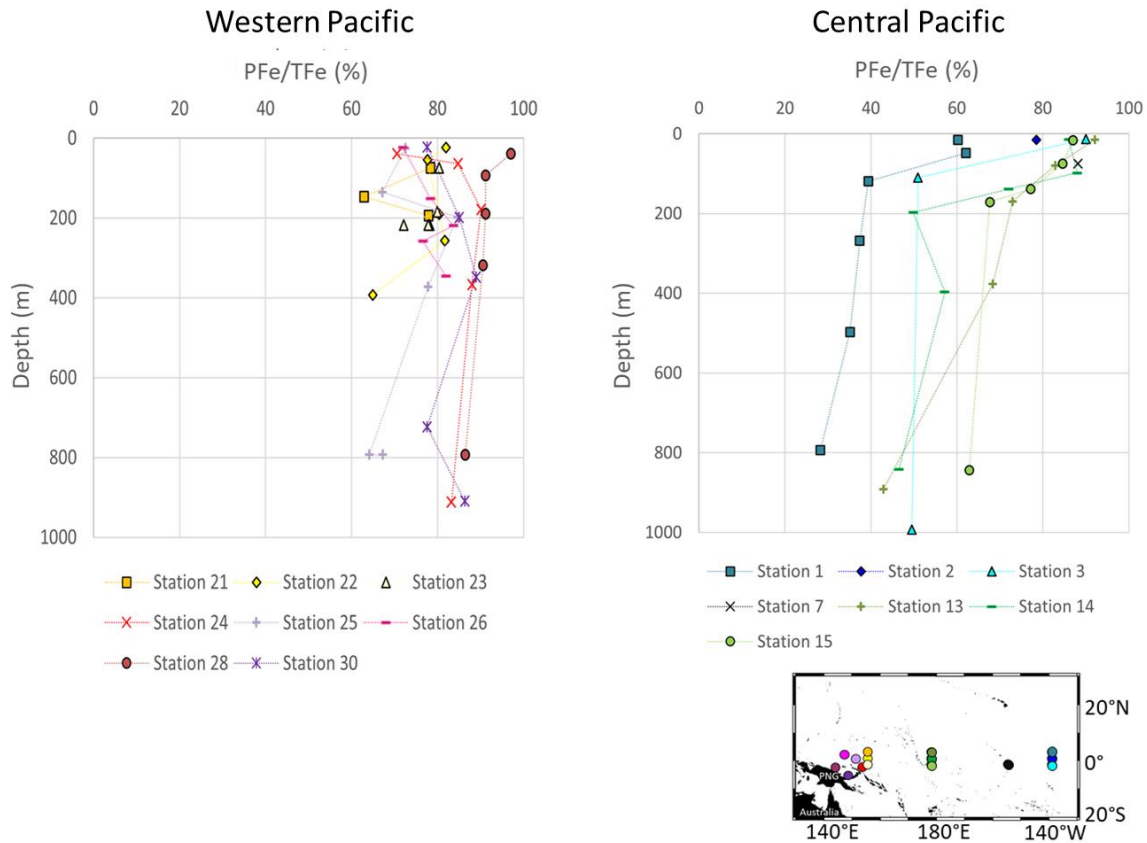
16.0

Average value

11.4 ± 6.6 (2SD)

903

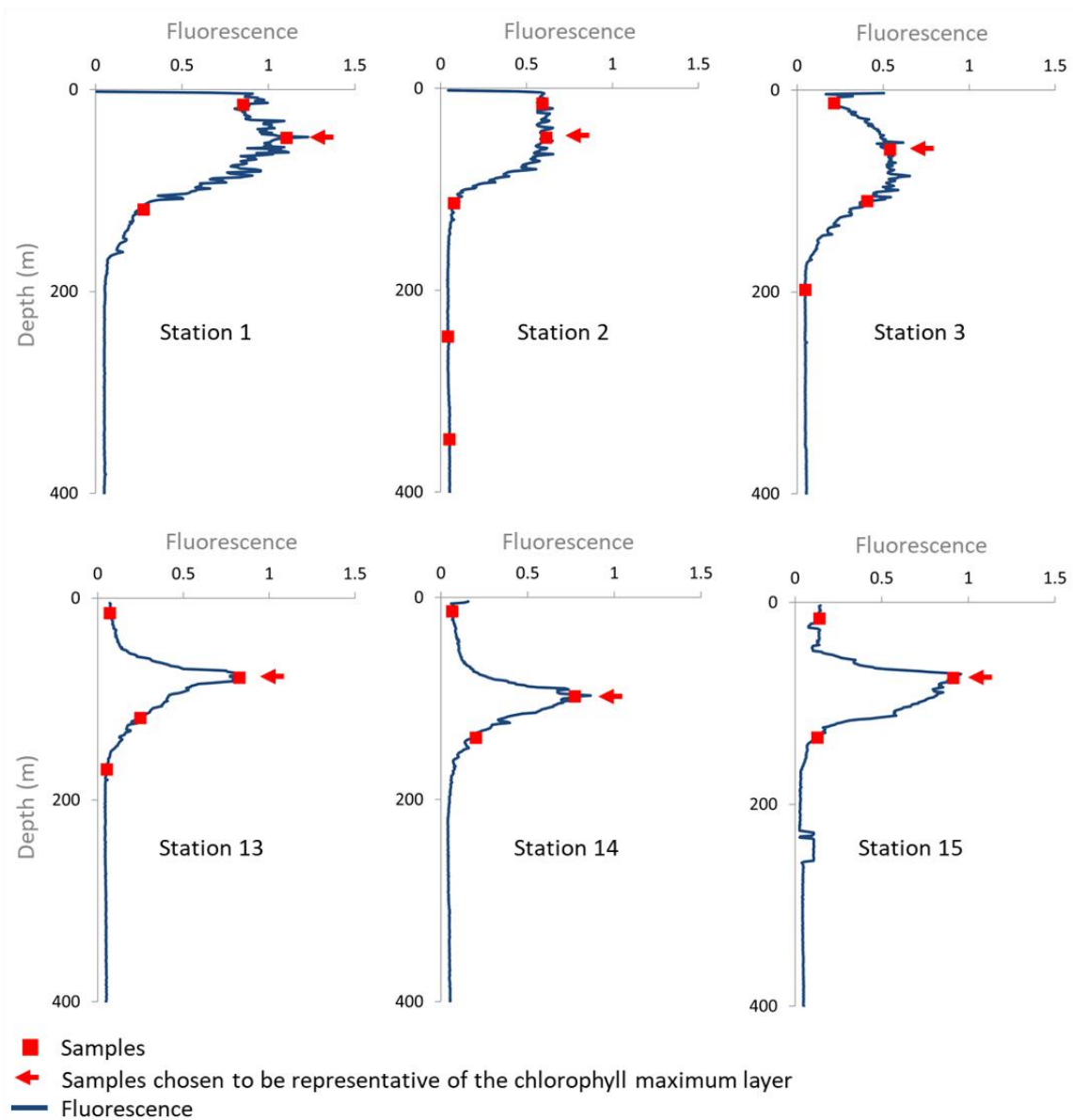
904 **Figure A1.** Fraction of particulate Fe (PFe) relative to total Fe (TFe) (% $\text{mol}\cdot\text{mol}^{-1}$) in the
905 western and central equatorial Pacific.



906

907

908 **Figure A2.** EUCFe cruise fluorescence profiles and sampling depth. Note that [the fluorescence](#)
909 [profiles were this fluorescence profiles have been](#) measured in the closest (in time) Niskin
910 rosette cast at the same station. Samples chosen as representative of the chlorophyll maximum
911 are shown by the (\leftarrow) symbol.



912

913 **Table A13.** Concentrations of particulate Fe and Al, dissolved Fe isotopic composition,
 914 estimated fractions of particulate phytoplanktonic and lithogenic Fe, isotopic composition of
 915 phytoplanktonic particulate Fe and the isotopic fractionation during biological uptake ($\Delta^{56}\text{Fe}_{\text{Phyto} - \text{DFe}}$)
 916 in the chlorophyll maximum layer. Uncertainties are reported as 95% confidence
 917 levels. Relative uncertainties for Fe and Al concentrations are 4.3 % (95% confidence level).

Station	Depth (m)	$\text{PFe}_{\text{total}}$ (nmol.kg^{-1})	$\delta^{56}\text{DFe}$ (‰)	PAI (nmol.kg^{-1})	$\text{PFe}_{\text{lithogenic}}$ (% mol.mol^{-1})	$\text{PFe}_{\text{phyto}}$ (% mol.mol^{-1})	$\delta^{56}\text{PFe}_{\text{phyto}}$ (‰)	$\Delta^{56}\text{Fe}_{\text{Phyto} - \text{DFe}}$ (‰)
Station 1	48	0.43	$+0.32 \pm 0.07$	0.53	61.7	38.3	$+0.54 \pm 0.19$	$+0.22 \pm 0.21$
Station 2	49	—	$+0.14 \pm 0.09$	6.65	—	—	—	—
Station 3	59	—	$+0.31 \pm 0.07$	0.67	—	—	—	—
Station 7	75	0.55	—	0.53	49.0	51.0	$+0.36 \pm 0.14$	—
Station 13	79	0.49	$+0.35 \pm 0.07$	0.15	15.2	84.8	$+0.30 \pm 0.12$	-0.05 ± 0.14
Station 14	98	0.43	$+0.58 \pm 0.07$	0.39	45.2	54.8	$+0.73 \pm 0.17$	$+0.15 \pm 0.19$
Station 15	75	0.27	—	0.22	40.4	59.6	$+0.46 \pm 0.12$	—

918

919 **DATA AVAILABILITY**

920 All the data used in this article are reported in Table 2. Fe concentration and isotope data
921 are available in the SEANOE data repository (<https://doi.org/10.17882/107774>, Lacan et al.,
922 2025) and ~~will also be~~ are included in the GEOTRACES Data Product.

923

924 **AUTHORS CONTRIBUTIONS**

925 J.W.M. was the principal investigator of the EUCFe cruise. F.L. conceived the iron
926 isotope work. M.L., C.P. and FL analyzed the samples. C.C., F.L. and M.L. wrote the article.
927 All co-authors reviewed the manuscript.

928

929 **COMPETING INTERESTS**

930 The authors declare that they have no conflict of interest.

931

932 **ACKNOWLEDGES**

933 Amandine Radic is very much thanked for having carried out a part of the isotope work.
934 Jérôme Chmeleff, Frédéric Candaudap, and Aurélie Marquet are thanked for their support with
935 the ICP-MS at the *Observatoire Midi-Pyrénées*. Oguz Yigiterhan and Joseph Resing for their
936 help around the Goflo bottles. The captain and the crew of the R/V *Kilo Moana* and especially
937 the marine technicians Gabe Foreman, and Daniel Fitzgerald are acknowledged. Jay Cullen
938 from University of Victoria is thanked for lending the trace-metal rosette. This study was
939 funded by French and USA public funds. The CNRS (French National Center for Scientific
940 Research) and the University of Toulouse (France) are thanked. The EUCFe expedition on the
941 R/V *Kilo Moana* was supported by NSF OCE 0425721 (USA, James W. Murray). The Fe
942 isotope project was funded by CNRS-INSU ISOFERIX project (France, François Lacan). [Tim
943 Conway and Matthias Sieber are acknowledged for their contributions to the GP15 and GP19
944 cruise data, and Derek Vance for his contributions to the GP19 cruise data; all were made
945 available through the GEOTRACES Intermediate Data Product. The three anonymous
946 reviewers are thanked for their comments, which allowed significantly improving the
947 manuscript.](#)

948

949 **FINANCIAL SUPPORT**

950 This study was funded by French and USA public funds. The CNRS (French National
951 Center for Scientific Research) and the University of Toulouse (France) are thanked. The
952 EUCFe expedition on the R/V *Kilo Moana* was supported by NSF OCE 0425721 (USA). The
953 Fe isotope project was funded par CNRS-INSU ISOFERIX project.

954

955

956 **REFERENCES**

957 Abadie, C., Lacan, F., Radic, A., Pradoux, C., and Poitrasson, F.: Iron isotopes reveal distinct
958 dissolved iron sources and pathways in the intermediate versus deep Southern Ocean, *P Natl A
959 Sci USA*, 114, 858–863, <https://doi.org/10.1073/pnas.1603107114>, 2017.

- 960 Auzende, J.-M., Ishibashi, J.-I., Beaudoin, Y., Charlou, J.-L., Delteil, J., Donval, J.-P., Fouquet,
961 Y., Ildefonse, B., Kimura, H., Nishio, Y., Radford-Knoery, J., and Ruðllan, E.: Extensive
962 magmatic and hydrothermal activity documented in Manus Basin, *Eos, Transactions American*
963 *Geophysical Union*, 81, 449–453, <https://doi.org/10.1029/00EO00331>, 2000.
- 964 Bacon, M. P. and Anderson, R. F.: Distribution of thorium isotopes between dissolved and
965 particulate forms in the deep sea, *J Geophys Res-Oceans*, 87, 2045–2056,
966 <https://doi.org/10.1029/JC087iC03p02045>, 1982.
- 967 [Baldacchino, G.: Islands, archipelagos and water: Insights from New Guinea, *MGRSD*, 29, 5–](https://doi.org/10.2478/mgrsd-2023-0050)
968 [10, *https://doi.org/10.2478/mgrsd-2023-0050*, 2024.](https://doi.org/10.2478/mgrsd-2023-0050)
- 969 Bennett, S. A., Rouxel, O., Schmidt, K., Garbe-Schönberg, D., Statham, P. J., and German, C.
970 R.: Iron isotope fractionation in a buoyant hydrothermal plume, 5°S Mid-Atlantic Ridge,
971 *Geochim Cosmochim Acta*, 73, 5619–5634, <https://doi.org/10.1016/j.gca.2009.06.027>, 2009.
- 972 Bergquist, B. A. and Boyle, E. A.: Iron isotopes in the Amazon River system: Weathering and
973 transport signatures, *Earth Planet Sc Lett*, 248, 54–68,
974 <https://doi.org/10.1016/j.epsl.2006.05.004>, 2006.
- 975 Bingham, F. M. and Lukas, R.: The distribution of intermediate water in the western equatorial
976 Pacific during January–February 1986, *Deep-Sea Res Pt I*, 42, 1545–1573,
977 [https://doi.org/10.1016/0967-0637\(95\)00064-D](https://doi.org/10.1016/0967-0637(95)00064-D), 1995.
- 978 [Bonnet, S., Biegala, I. C., Dutrieux, P., Slemmons, L. O., and Capone, D. G.: Nitrogen fixation](https://doi.org/10.1029/2008GB003439)
979 [in the western equatorial Pacific: Rates, diazotrophic cyanobacterial size class distribution, and](https://doi.org/10.1029/2008GB003439)
980 [biogeochemical significance, *Global Biogeochemical Cycles*, 23,](https://doi.org/10.1029/2008GB003439)
981 [*https://doi.org/10.1029/2008GB003439*, 2009.](https://doi.org/10.1029/2008GB003439)
- 982 Bostock, H. C., Opdyke, B. N., and Williams, M. J. M.: Characterising the intermediate depth
983 waters of the Pacific Ocean using $\delta^{13}\text{C}$ and other geochemical tracers, *Deep-Sea Res Pt I*, 57,
984 847–859, <https://doi.org/10.1016/j.dsr.2010.04.005>, 2010.
- 985 Boyle, E. A., John, S., Abouchami, W., Adkins, J. F., Echegoyen-Sanz, Y., Ellwood, M., Flegal,
986 A. R., Fornace, K., Gallon, C., Galer, S., Gault-Ringold, M., Lacan, F., Radic, A., Rehkamper,
987 M., Rouxel, O., Sohrin, Y., Stirling, C., Thompson, C., Vance, D., Xue, Z., and Zhao, Y.:
988 GEOTRACES IC1 (BATS) contamination-prone trace element isotopes Cd, Fe, Pb, Zn, Cu,
989 and Mo intercalibration, *Limno Oceanogr-Meth*, 10, 653–665,
990 <https://doi.org/10.4319/lom.2012.10.653>, 2012.
- 991 Butt, J. and Lindstrom, E.: Currents off the east coast of New Ireland, Papua New Guinea, and
992 their relevance to regional undercurrents in the western equatorial Pacific Ocean, *J Geophys*
993 *Res-Oceans*, 99, 12503–12514, <https://doi.org/10.1029/94JC00399>, 1994.
- 994 Camin, C., Lacan, F., Pradoux, C., Labatut, M., Johansen, A., and Murray, J. W.: Iron isotopes
995 suggest significant aerosol dissolution over the Pacific Ocean, *Atmos Chem Phys*, 25, 8213–
996 8228, <https://doi.org/10.5194/acp-25-8213-2025>, 2025.
- 997 Cardinal, D., Dehairs, F., Cattaldo, T., and André, L.: Geochemistry of suspended particles in
998 the Subantarctic and Polar Frontal zones south of Australia: Constraints on export and advection
999 processes, *J Geophys Res-Oceans*, 106, 31637–31656, <https://doi.org/10.1029/2000JC000251>,
1000 2001.
- 1001 Ccanccapa-Cartagena, A., Chavez-Gonzales, F. D., Paredes, B., Vera, C., Gutierrez, G.,
1002 Valencia, R., Lucia Paz Alcázar, A., Zyaykina, N. N., Filley, T. R., and Jafvert, C. T.: Seasonal
1003 differences in trace metal concentrations in the major rivers of the hyper-arid southwestern

- 1004 Andes basins of Peru, *J Environ Manage*, 344, 118493,
1005 <https://doi.org/10.1016/j.jenvman.2023.118493>, 2023.
- 1006 Chavez, F. P., Buck, K. R., and Barber, R. T.: Phytoplankton taxa in relation to primary
1007 production in the equatorial Pacific, *Deep Sea Research Part A. Oceanographic Research*
1008 *Papers*, 37, 1733–1752, [https://doi.org/10.1016/0198-0149\(90\)90074-6](https://doi.org/10.1016/0198-0149(90)90074-6), 1990.
- 1009 Chisholm, S. W. and Morel, F. M. M.: What controls phytoplankton production in nutrient-rich
1010 areas of the open sea?, in: *Limnology and Oceanography*, American Society of Limnology and
1011 *Oceanography Symposium*, San-Marcos, California, U1507–U1511, 1991.
- 1012 Coale, K. H., Fitzwater, S. E., Gordon, R. M., Johnson, K. S., and Barber, R. T.: Control of
1013 community growth and export production by upwelled iron in the equatorial Pacific Ocean,
1014 *Nature*, 379, 621–624, <https://doi.org/10.1038/379621a0>, 1996.
- 1015 Cohen, N. R., Noble, A. E., Moran, D. M., McIlvin, M. R., Goepfert, T. J., Hawco, N. J.,
1016 German, C. R., Horner, T. J., Lamborg, C. H., McCrow, J. P., Allen, A. E., and Saito, M. A.:
1017 Hydrothermal trace metal release and microbial metabolism in the northeastern Lau Basin of
1018 the South Pacific Ocean, *Biogeosciences*, 18, 5397–5422, [https://doi.org/10.5194/bg-18-5397-](https://doi.org/10.5194/bg-18-5397-2021)
1019 2021, 2021.
- 1020 Conway, T. M. and John, S. G.: Quantification of dissolved iron sources to the North Atlantic
1021 Ocean, *Nature*, 511, 212–215, <https://doi.org/10.1038/nature13482>, 2014.
- 1022 Conway, T. M., John, S. G., and Lacan, F.: Intercomparison of dissolved iron isotope profiles
1023 from reoccupation of three GEOTRACES stations in the Atlantic Ocean, *Mar Chem*, 183, 50–
1024 61, <https://doi.org/10.1016/j.marchem.2016.04.007>, 2016.
- 1025 Cravatte, S., Kestenare, E., Marin, F., Dutrieux, P., and Firing, E.: Subthermocline and
1026 Intermediate Zonal Currents in the Tropical Pacific Ocean: Paths and Vertical Structure, *J Phys*
1027 *Oceanogr*, 47, 2305–2324, <https://doi.org/10.1175/JPO-D-17-0043.1>, 2017.
- 1028 Criss, R. E.: *Principles of Stable Isotope Distribution*, Oxford University Press, Oxford, New
1029 York, 264 pp., ISBN 978-0-19-756119-5, 1999.
- 1030 Dammshäuser, A.: Distribution and behavior of the lithogenic tracers aluminium and titanium
1031 in the upper water column of the Atlantic Ocean, Faculty of Mathematics and Natural Sciences
1032 Christian-Albrechts-Universität zu Kiel, [https://nbn-resolving.org/urn:nbn:de:gbv:8-diss-](https://nbn-resolving.org/urn:nbn:de:gbv:8-diss-81211)
1033 81211 (last access:16 November 2024), 2012.
- 1034 Delcroix, T., Eldin, G., Radenac, M.-H., Toole, J., and Firing, E.: Variation of the western
1035 equatorial Pacific Ocean, 1986–1988, *Journal of Geophysical Research: Oceans*, 97, 5423–
1036 5445, <https://doi.org/10.1029/92JC00127>, 1992.
- 1037 Ellwood, M. J., Hutchins, D. A., Lohan, M. C., Milne, A., Nasemann, P., Nodder, S. D., Sander,
1038 S. G., Strzepek, R., Wilhelm, S. W., and Boyd, P. W.: Iron stable isotopes track pelagic iron
1039 cycling during a subtropical phytoplankton bloom, *P Natl Acad Sci USA*, 112, E15–E20,
1040 <https://doi.org/10.1073/pnas.1421576112>, 2015.
- 1041 Ellwood, M. J., Strzepek, R. F., Strutton, P. G., Trull, T. W., Fourquez, M., and Boyd, P. W.:
1042 Distinct iron cycling in a Southern Ocean eddy, *Nat Commun*, 11, 825,
1043 <https://doi.org/10.1038/s41467-020-14464-0>, 2020.
- 1044 Emery, W. J. and Meincke, J.: Global water masses : summary and review, *Oceanol Acta*, 9,
1045 383–391, ISSN 0399-1784, 1986.

- 1046 Fantle, M. S. and DePaolo, D. J.: Iron isotopic fractionation during continental weathering,
1047 *Earth Planet Sc Lett*, 228, 547–562, <https://doi.org/10.1016/j.epsl.2004.10.013>, 2004.
- 1048 Fiedler, P. C. and Talley, L. D.: Hydrography of the eastern tropical Pacific: A review, *Prog*
1049 *Oceanogr*, 69, 143–180, <https://doi.org/10.1016/j.pocean.2006.03.008>, 2006.
- 1050 Fine, R. A., Lukas, R., Bingham, F. M., Warner, M. J., and Gammon, R. H.: The western
1051 equatorial Pacific: A water mass crossroads, *Journal of Geophysical Research: Oceans*, 99,
1052 25063–25080, <https://doi.org/10.1029/94JC02277>, 1994.
- 1053 Fitzsimmons, J. N., John, S. G., Marsay, C. M., Hoffman, C. L., Nicholas, S. L., Toner, B. M.,
1054 German, C. R., and Sherrell, R. M.: Iron persistence in a distal hydrothermal plume supported
1055 by dissolved–particulate exchange, *Nature Geosci*, 10, 195–201,
1056 <https://doi.org/10.1038/ngeo2900>, 2017.
- 1057 Flament, P., Mattielli, N., Aimoz, L., Choël, M., Deboudt, K., Jong, J. de, Rimetz-Planchon, J.,
1058 and Weis, D.: Iron isotopic fractionation in industrial emissions and urban aerosols,
1059 *Chemosphere*, 73, 1793–1798, <https://doi.org/10.1016/j.chemosphere.2008.08.042>, 2008.
- 1060 Frank, M., Eisenhauer, A., Bonn, W. J., Walter, P., Grobe, H., Kubik, P. W., Dittrich-Hannen,
1061 B., and Mangini, A.: Sediment redistribution versus paleoproductivity change: Weddell Sea
1062 margin sediment stratigraphy and biogenic particle flux of the last 250,000 years deduced from
1063 ²³⁰Thex, ¹⁰Be and biogenic barium profiles, *Earth Planet Sc Lett*, 136, 559–573,
1064 [https://doi.org/10.1016/0012-821X\(95\)00161-5](https://doi.org/10.1016/0012-821X(95)00161-5), 1995.
- 1065 ~~[GEOTRACES Intermediate Data Product Group: The GEOTRACES Intermediate Data](#)~~
1066 ~~[Product 2021v2 \(IDP2021v2\) \(2\), \[https://doi.org/10.5285/ff46f034-f47c-05f9-e053-\]\(https://doi.org/10.5285/ff46f034-f47c-05f9-e053-6e86abc0de7e\)](#)~~
1067 ~~[6e86abc0de7e](#), [data set], 2023.~~
- 1068 [GEOTRACES Intermediate Data Product Group: The GEOTRACES Intermediate Data](#)
1069 [Product 2025 \(IDP2025\)](#), <https://doi:10.5285/42c92148-8d03-8be6-e063-7086abc09f0c>, [data
1070 set], 2025.
- 1071 Germineaud, C., Ganachaud, A., Sprintall, J., Cravatte, S., Eldin, G., Albery, M. S., and Privat,
1072 E.: Pathways and Water Mass Properties of the Thermocline and Intermediate Waters in the
1073 Solomon Sea, *J Phys Oceanogr*, 46, 3031–3049, <https://doi.org/10.1175/JPO-D-16-0107.1>,
1074 2016.
- 1075 Gordon, R. M., Coale, K. H., and Johnson, K. S.: Iron distributions in the equatorial Pacific:
1076 Implications for new production, *Limnol Oceanogr*, 42, 419–431,
1077 <https://doi.org/10.4319/lo.1997.42.3.0419>, 1997.
- 1078 Grenier, M.: Le rôle du pacifique tropical sud-ouest dans la fertilisation du pacifique équatorial :
1079 couplage dynamique et multi-traceur, *These de doctorat, Toulouse 3*, 205 pp.,
1080 <https://theses.hal.science/tel-00876092> (last access: 4 April 2024), 2012.
- 1081 Grenier, M., Cravatte, S., Blanke, B., Menkes, C., Koch-Larrouy, A., Durand, F., Melet, A.,
1082 and Jeandel, C.: From the western boundary currents to the Pacific Equatorial Undercurrent:
1083 Modeled pathways and water mass evolutions, *Journal of Geophysical Research: Oceans*, 116,
1084 <https://doi.org/10.1029/2011JC007477>, 2011.
- 1085 Grenier, M., Jeandel, C., Lacan, F., Vance, D., Venchiarutti, C., Cros, A., and Cravatte, S.:
1086 From the subtropics to the central equatorial Pacific Ocean: Neodymium isotopic composition
1087 and rare earth element concentration variations, *J Geophys Res-Oceans*, 118, 592–618,
1088 <https://doi.org/10.1029/2012JC008239>, 2013.

- 1089 Hayes, J.: An Introduction to Isotopic Calculations, Woods Hole Oceanographic Institution,
1090 <https://doi.org/10.1575/1912/27058>, 2004.
- 1091 He, Y., Kadko, D. C., Stephens, M. P., Sheridan, M. T., Buck, C. S., Marsay, C. M., Landing,
1092 W. M., Zheng, M., and Liu, P.: Constraining aerosol deposition over the global ocean, *Nat.*
1093 *Geosci.*, 18, 966–974, <https://doi.org/10.1038/s41561-025-01785-2>, 2025.
- 1094 Homoky, W. B., Severmann, S., Mills, R. A., Statham, P. J., and Fones, G. R.: Pore-fluid Fe
1095 isotopes reflect the extent of benthic Fe redox recycling: Evidence from continental shelf and
1096 deep-sea sediments, *Geology*, 37, 751–754, <https://doi.org/10.1130/G25731A.1>, 2009.
- 1097 Homoky, W. B., Conway, T. M., John, S. G., König, D., Deng, F., Tagliabue, A., and Mills, R.
1098 A.: Iron colloids dominate sedimentary supply to the ocean interior, *P Natl Acad Sci USA*, 118,
1099 e2016078118, <https://doi.org/10.1073/pnas.2016078118>, 2021.
- 1100 Ingri, J., Malinovsky, D., Rodushkin, I., Baxter, D. C., Widerlund, A., Andersson, P.,
1101 Gustafsson, Ö., Forsling, W., and Öhlander, B.: Iron isotope fractionation in river colloidal
1102 matter, *Earth Planet Sc Lett*, 245, 792–798, <https://doi.org/10.1016/j.epsl.2006.03.031>, 2006.
- 1103 John, S. G., Boyle, E. A., Cunningham, B. R., Fu, F.-X., Greene, S., Hodierne, C., Hutchins, D.
1104 A., Kavner, A., King, A. L., Rosenberg, A. D., Saito, M. A., and Wasson, A.: Kinetic Isotope
1105 Effects During Reduction of Fe(III) to Fe(II): Large Normal and Inverse Isotope Effects for
1106 Abiotic Reduction and Smaller Fractionations by Phytoplankton in Culture, *Geochemistry,*
1107 *Geophysics, Geosystems*, 25, e2023GC010952, <https://doi.org/10.1029/2023GC010952>, 2024.
- 1108 John, S. G., Mendez, J., Moffett, J., and Adkins, J.: The flux of iron and iron isotopes from San
1109 Pedro Basin sediments, *Geochim Cosmochim Ac*, 93, 14–29,
1110 <https://doi.org/10.1016/j.gca.2012.06.003>, 2012.
- 1111 John, S. G., Helgoe, J., Townsend, E., Weber, T., DeVries, T., Tagliabue, A., Moore, K., Lam,
1112 P., Marsay, C. M., and Till, C.: Biogeochemical cycling of Fe and Fe stable isotopes in the
1113 Eastern Tropical South Pacific, *Mar Chem*, 201, 66–76,
1114 <https://doi.org/10.1016/j.marchem.2017.06.003>, 2018.
- 1115 Johnson, G. C., Sloyan, B. M., Kessler, W. S., and McTaggart, K. E.: Direct measurements of
1116 upper ocean currents and water properties across the tropical Pacific during the 1990s, *Progress*
1117 *in Oceanography*, 52, 31–61, [https://doi.org/10.1016/S0079-6611\(02\)00021-6](https://doi.org/10.1016/S0079-6611(02)00021-6), 2002.
- 1118 Johnson, Z., Shyam, R., Ritchie, A., Mioni, C., Lance, V., Murray, J., and Zinser, E.: The effect
1119 of iron- and light-limitation on phytoplankton communities of deep chlorophyll maxima of the
1120 western Pacific Ocean, *Journal of Marine Research*, 68, 2010.
- 1121 Kadko, D., Landing, W. M., and Buck, C. S.: Quantifying Atmospheric Trace Element
1122 Deposition Over the Ocean on a Global Scale With Satellite Rainfall Products, *Geophysical*
1123 *Research Letters*, 47, e2019GL086357, <https://doi.org/10.1029/2019GL086357>, 2020.
- 1124 Kashino, Y., Aoyama, M., Kawano, T., Hendiarti, N., Syaefudin, Anantasena, Y., Muneyama,
1125 K., and Watanabe, H.: The water masses between Mindanao and New Guinea, *Journal of*
1126 *Geophysical Research: Oceans*, 101, 12391–12400, <https://doi.org/10.1029/95JC03797>, 1996.
- 1127 Kashino, Y., Ueki, I., Kuroda, Y., and Purwandani, A.: Ocean variability North of New Guinea
1128 derived from TRITON buoy data, *J Oceanogr*, 63, 545–559, [https://doi.org/10.1007/s10872-](https://doi.org/10.1007/s10872-007-0049-y)
1129 [007-0049-y](https://doi.org/10.1007/s10872-007-0049-y), 2007.

- 1130 Kaupp, L. J., Measures, C. I., Selph, K. E., and Mackenzie, F. T.: The distribution of dissolved
1131 Fe and Al in the upper waters of the Eastern Equatorial Pacific, *Deep-Sea Res Pt II*, 58, 296–
1132 310, <https://doi.org/10.1016/j.dsr2.2010.08.009>, 2011.
- 1133 Kineke, G. C., Woolfe, K. J., Kuehl, S. A., Milliman, J. D., Dellapenna, T. M., and Purdon, R.
1134 G.: Sediment export from the Sepik River, Papua New Guinea: evidence for a divergent
1135 sediment plume, *Cont Shelf Res*, 20, 2239–2266, [https://doi.org/10.1016/S0278-4343\(00\)00069-8](https://doi.org/10.1016/S0278-4343(00)00069-8), 2000.
- 1137 Klar, J. K., Schlosser, C., Milton, J. A., Woodward, E. M. S., Lacan, F., Parkinson, I. J.,
1138 Achterberg, E. P., and James, R. H.: Sources of dissolved iron to oxygen minimum zone waters
1139 on the Senegalese continental margin in the tropical North Atlantic Ocean: Insights from iron
1140 isotopes, *Geochim Cosmochim Acta*, 236, 60–78, <https://doi.org/10.1016/j.gca.2018.02.031>,
1141 2018.
- 1142 Kuehl, S. A., Brunskill, G. J., Burns, K., Fugate, D., Kniskern, T., and Meneghini, L.: Nature
1143 of sediment dispersal off the Sepik River, Papua New Guinea: preliminary sediment budget and
1144 implications for margin processes, *Cont Shelf Res*, 24, 2417–2429,
1145 <https://doi.org/10.1016/j.csr.2004.07.016>, 2004.
- 1146 Kurisu, M., Sakata, K., Miyamoto, C., Takaku, Y., Iizuka, T., and Takahashi, Y.: Variation of
1147 Iron Isotope Ratios in Anthropogenic Materials Emitted through Combustion Processes, *Chem*
1148 *Lett*, 45, 970–972, <https://doi.org/10.1246/cl.160451>, 2016.
- 1149 Labatut, M., Lacan, F., Pradoux, C., Chmeleff, J., Radic, A., Murray, J. W., Poitrasson, F.,
1150 Johansen, A. M., and Thil, F.: Iron sources and dissolved-particulate interactions in the seawater
1151 of the Western Equatorial Pacific, iron isotope perspectives, *Global Biogeochem Cy*, 28, 1044–
1152 1065, <https://doi.org/10.1002/2014GB004928>, 2014.
- 1153 Lacan, F. and Jeandel, C.: Tracing Papua New Guinea imprint on the central Equatorial Pacific
1154 Ocean using neodymium isotopic compositions and Rare Earth Element patterns, *Earth Planet*
1155 *Sc Lett*, 186, 497–512, [https://doi.org/10.1016/S0012-821X\(01\)00263-1](https://doi.org/10.1016/S0012-821X(01)00263-1), 2001.
- 1156 [Lacan, F. and Jeandel, C.: Neodymium isotopes as a new tool for quantifying exchange fluxes
1157 at the continent–ocean interface, *Earth and Planetary Science Letters*, 232, 245–257,
1158 <https://doi.org/10.1016/j.epsl.2005.01.004>, 2005.](#)
- 1159 Lacan, F., Radic, A., Jeandel, C., Poitrasson, F., Sarthou, G., Pradoux, C., and Freydier, R.:
1160 Measurement of the isotopic composition of dissolved iron in the open ocean, *Geophys Res*
1161 *Lett*, 35, L24610, <https://doi.org/10.1029/2008GL035841>, 2008.
- 1162 Lacan, F., Radic, A., Labatut, M., Jeandel, C., Poitrasson, F., Sarthou, G., Pradoux, C.,
1163 Chmeleff, J., and Freydier, R.: High-Precision Determination of the Isotopic Composition of
1164 Dissolved Iron in Iron Depleted Seawater by Double Spike Multicollector-ICPMS, *Anal Chem*,
1165 82, 7103–7111, <https://doi.org/10.1021/ac1002504>, 2010.
- 1166 Lacan, F., Artigue, L., Klar, J. K., Pradoux, C., Chmeleff, J., and Freydier, R.: Interferences
1167 and Matrix Effects on Iron Isotopic Composition Measurements by ^{57}Fe - ^{58}Fe Double-Spike
1168 Multi-Collector Inductively Coupled Plasma Mass Spectrometry; the Importance of Calcium
1169 and Aluminum Interferences, *Front Environ Chem*, 2,
1170 <https://doi.org/10.3389/fenvc.2021.692025>, 2021.
- 1171 Lacan, F., Pradoux, C., Dutrieux, P., Murray, J. W., Johansen, A., Radic, A., and Labatut, M.:
1172 CTD, dissolved oxygen concentrations, iron concentrations and isotopic compositions in the
1173 filtered seawater, seawater suspended particles and aerosols, during the EUCFe cruise,

- 1174 KM0625, in the Equatorial Pacific Ocean, SEANOE [data set],
1175 <https://doi.org/10.17882/107774>, 2025.
- 1176 Landry, M. R., Kirshtein, J., and Constantinou, J.: Abundances and distributions of
1177 picoplankton populations in the central equatorial Pacific from 12°N to 12°S, 140°W, *Deep Sea*
1178 *Research Part II: Topical Studies in Oceanography*, 43, 871–890, [https://doi.org/10.1016/0967-](https://doi.org/10.1016/0967-0645(96)00018-5)
1179 [0645\(96\)00018-5](https://doi.org/10.1016/0967-0645(96)00018-5), 1996.
- 1180 Lory, C., Van Wambeke, F., Fourquez, M., Barani, A., Guieu, C., Tilliette, C., Marie, D.,
1181 Nunige, S., Berman-Frank, I., and Bonnet, S.: Assessing the contribution of diazotrophs to
1182 microbial Fe uptake using a group specific approach in the Western Tropical South Pacific
1183 Ocean, *ISME Commun*, 2, 41, <https://doi.org/10.1038/s43705-022-00122-7>, 2022.
- 1184 Mackey, D. J., O’Sullivan, J. E. Os., and Watson, R. J.: Iron in the western Pacific: a riverine
1185 or hydrothermal source for iron in the Equatorial Undercurrent?, *Deep-Sea Res Pt I*, 49, 877–
1186 893, [https://doi.org/10.1016/S0967-0637\(01\)00075-9](https://doi.org/10.1016/S0967-0637(01)00075-9), 2002.
- 1187 Marchetti, A., Varela, D. E., Lance, V. P., Lance, V. P., Palmucci, M., Giordano, M., and
1188 Virginia Armbrust, E.: Iron and silicic acid effects on phytoplankton productivity, diversity,
1189 and chemical composition in the central equatorial Pacific Ocean, *Limnology and*
1190 *Oceanography*, 55, 11–29, <https://doi.org/10.4319/lo.2010.55.1.0011>, 2010.
- 1191 Marsay, C. M., Lam, P. J., Heller, M. I., Lee, J.-M., and John, S. G.: Distribution and isotopic
1192 signature of ligand-leachable particulate iron along the GEOTRACES GP16 East Pacific Zonal
1193 Transect, *Mar Chem*, 201, 198–211, <https://doi.org/10.1016/j.marchem.2017.07.003>, 2018.
- 1194 Martin, J. H.: Iron as a Limiting Factor in Oceanic Productivity, in: *Primary Productivity and*
1195 *Biogeochemical Cycles in the Sea*, edited by: Falkowski, P. G., Woodhead, A. D., and Vivirito,
1196 K., Springer, Boston, MA, 123–137, https://doi.org/10.1007/978-1-4899-0762-2_8, 1992.
- 1197 McCartney, M. S.: Subantarctic Mode Water, Woods Hole Oceanographic Institution
1198 Contribution 3773, 103–119,
1199 <https://www.whoi.edu/science/PO/people/mmccartney/pdfs/McCartney77.pdf> (last access: 15
1200 January 2025), 1977.
- 1201 McManus, J., Berelson, W. M., Hammond, D. E., and Klinkhammer, G. P.: Barium Cycling in
1202 the North Pacific: Implications for the Utility of Ba as a Paleoproductivity and Paleoalkalinity
1203 Proxy, *Paleoceanography*, 14, 53–61, <https://doi.org/10.1029/1998PA900007>, 1999.
- 1204 Milliman, J. D.: Sediment discharge to the ocean from small mountainous rivers: The New
1205 Guinea example, *Geo-Mar Lett*, 15, 127–133, <https://doi.org/10.1007/BF01204453>, 1995.
- 1206 Milliman, J. D. and Syvitski, J. P. M.: Geomorphic/Tectonic Control of Sediment Discharge to
1207 the Ocean: The Importance of Small Mountainous Rivers, *The Journal of Geology*, 100, 525–
1208 544, <https://doi.org/10.1086/629606>, 1992.
- 1209 Milliman, J. D., Farnsworth, K. L., and Albertin, C. S.: Flux and fate of fluvial sediments
1210 leaving large islands in the East Indies, *J Sea Res*, 41, 97–107, [https://doi.org/10.1016/S1385-](https://doi.org/10.1016/S1385-1101(98)00040-9)
1211 [1101\(98\)00040-9](https://doi.org/10.1016/S1385-1101(98)00040-9), 1999.
- 1212 Morel, F. M. M., Lam, P. J., and Saito, M. A.: Trace Metal Substitution in Marine
1213 Phytoplankton, *Annu Rev Earth Pl Sc*, 48, 491–517, [https://doi.org/10.1146/annurev-earth-](https://doi.org/10.1146/annurev-earth-053018-060108)
1214 [053018-060108](https://doi.org/10.1146/annurev-earth-053018-060108), 2020.
- 1215 Mulholland, D. S., Poitrasson, F., Shirokova, L. S., González, A. G., Pokrovsky, O. S.,
1216 Boaventura, G. R., and Vieira, L. C.: Iron isotope fractionation during Fe(II) and Fe(III)

- 1217 adsorption on cyanobacteria, *Chemical Geology*, 400, 24–33,
1218 <https://doi.org/10.1016/j.chemgeo.2015.01.017>, 2015.
- 1219 Murray, J. W., Barber, R. T., Roman, M. R., Bacon, M. P., and Feely, R. A.: Physical and
1220 Biological Controls on Carbon Cycling in the Equatorial Pacific, *Science*, 266, 58–65,
1221 <https://doi.org/10.1126/science.266.5182.58>, 1994.
- 1222 Murray, R. W., Leinen, M., and Isern, A. R.: Biogenic flux of Al to sediment in the central
1223 equatorial Pacific Ocean: Evidence for increased productivity during glacial periods,
1224 *Paleoceanography*, 8, 651–670, <https://doi.org/10.1029/93PA02195>, 1993.
- 1225 Nozaki, Y. and Alibo, D. S.: Dissolved rare earth elements in the Southern Ocean, southwest
1226 of Australia: Unique patterns compared to the South Atlantic data, *Geochem J*, 37, 47–62,
1227 <https://doi.org/10.2343/geochemj.37.47>, 2003.
- 1228 Nozaki, Y., Yang, H.-S., and Yamada, M.: Scavenging of thorium in the ocean, *J Geophys Res-*
1229 *Oceans*, 92, 772–778, <https://doi.org/10.1029/JC092iC01p00772>, 1987.
- 1230 Philander, S. G. H.: equatorial undercurrent: Measurements and theories, *Rev Geophys*, 11,
1231 513–570, <https://doi.org/10.1029/RG011i003p00513>, 1973.
- 1232 Pickard, G. L. and Emery, W. J.: *Descriptive Physical Oceanography*, Elsevier, 348 pp., ISBN
1233 978-0-7506-2759-7, 1990.
- 1234 Poitrasson, F.: On the iron isotope homogeneity level of the continental crust, *Chem Geol*, 235,
1235 195–200, <https://doi.org/10.1016/j.chemgeo.2006.06.010>, 2006.
- 1236 Pollard, R. T., Griffiths, M. J., Cunningham, S. A., Read, J. F., Pérez, F. F., and Ríos, A. F.:
1237 Vivaldi 1991 - A study of the formation, circulation and ventilation of Eastern North Atlantic
1238 Central Water, *Prog Oceanogr*, [https://doi.org/10.1016/S0079-6611\(96\)00008-0](https://doi.org/10.1016/S0079-6611(96)00008-0), 1996.
- 1239 Qu, T. and Lindstrom, E. J.: A Climatological Interpretation of the Circulation in the Western
1240 South Pacific, *J Phys Oceanogr*, 32, 2492–2508, [https://doi.org/10.1175/1520-0485\(2002\)032<2492:ACIOTC>2.0.CO;2](https://doi.org/10.1175/1520-0485(2002)032<2492:ACIOTC>2.0.CO;2), 2002.
- 1242 Qu, T. and Lindstrom, E. J.: Northward Intrusion of Antarctic Intermediate Water in the
1243 Western Pacific, *J Phys Oceanogr*, 34, 2104–2118, [https://doi.org/10.1175/1520-0485\(2004\)034<2104:NIOAIW>2.0.CO;2](https://doi.org/10.1175/1520-0485(2004)034<2104:NIOAIW>2.0.CO;2), 2004.
- 1245 Qu, T., Gao, S., Fukumori, I., Fine, R. A., and Lindstrom, E. J.: Origin and Pathway of
1246 Equatorial 13°C Water in the Pacific Identified by a Simulated Passive Tracer and Its Adjoint,
1247 *J Phys Oceanogr*, 39, 1836–1853, <https://doi.org/10.1175/2009JPO4045.1>, 2009.
- 1248 Radic, A., Lacan, F., and Murray, J. W.: Iron isotopes in the seawater of the equatorial Pacific
1249 Ocean: New constraints for the oceanic iron cycle, *Earth Planet Sc Lett*, 306, 1–10,
1250 <https://doi.org/10.1016/j.epsl.2011.03.015>, 2011.
- 1251 Renagi, O., Ridd, P., and Stieglitz, T.: Quantifying the suspended sediment discharge to the
1252 ocean from the Markham River, Papua New Guinea, *Cont Shelf Res*, 30, 1030–1041,
1253 <https://doi.org/10.1016/j.csr.2010.01.015>, 2010.
- 1254 [Resing, J. A., Sedwick, P. N., German, C. R., Jenkins, W. J., Moffett, J. W., Sohst, B. M., and Tagliabue, A.: Basin-scale transport of hydrothermal dissolved metals across the South Pacific Ocean, *Nature*, 523, 200–203, <https://doi.org/10.1038/nature14577>, 2015.](https://doi.org/10.1038/nature14577)

- 1257 Rodgers, K. B., Blanke, B., Madec, G., Aumont, O., Ciais, P., and Dutay, J.-C.: Extratropical
1258 sources of Equatorial Pacific upwelling in an OGCM, *Geophys Res Lett*, 30,
1259 <https://doi.org/10.1029/2002GL016003>, 2003.
- 1260 Rousseau, T. C. C., Sonke, J. E., Chmeleff, J., van Beek, P., Souhaut, M., Boaventura, G.,
1261 Seyler, P., and Jeandel, C.: Rapid neodymium release to marine waters from lithogenic
1262 sediments in the Amazon estuary, *Nat Commun*, 6, 7592, <https://doi.org/10.1038/ncomms8592>,
1263 2015.
- 1264 Rouxel, O., Shanks, W. C., Bach, W., and Edwards, K. J.: Integrated Fe- and S-isotope study
1265 of seafloor hydrothermal vents at East Pacific Rise 9–10°N, *Chemical Geology*, 252, 214–227,
1266 <https://doi.org/10.1016/j.chemgeo.2008.03.009>, 2008.
- 1267 Rudnick, R. L. and Gao, S.: 4.1 - Composition of the Continental Crust, in: *Treatise on*
1268 *Geochemistry (Second Edition)*, edited by: Holland, H. D. and Turekian, K. K., Elsevier,
1269 Oxford, 1–51, <https://doi.org/10.1016/B978-0-08-095975-7.00301-6>, 2014.
- 1270 Ryan, J. P., Ueki, I., Chao, Y., Zhang, H., Polito, P. S., and Chavez, F. P.: Western Pacific
1271 modulation of large phytoplankton blooms in the central and eastern equatorial Pacific, *Journal*
1272 *of Geophysical Research: Biogeosciences*, 111, <https://doi.org/10.1029/2005JG000084>, 2006.
- 1273 Sarthou, G., Bucciarelli, E., Quéroué, F., Lacan, F., Planquette, H., Pham, V. Q., Grand, M.,
1274 Pradoux, C., Rodier, M., Bonnet, S., Eldin, G., Cravatte, S., Jeandel, C., and Ganachaud, A.:
1275 Dissolved iron distribution and budget in the Solomon Sea, *Marine Chemistry*, 273, 104567,
1276 <https://doi.org/10.1016/j.marchem.2025.104567>, 2025.
- 1277 Severmann, S., Johnson, C. M., Beard, B. L., German, C. R., Edmonds, H. N., Chiba, H., and
1278 Green, D. R. H.: The effect of plume processes on the Fe isotope composition of hydrothermally
1279 derived Fe in the deep ocean as inferred from the Rainbow vent site, Mid-Atlantic Ridge,
1280 36°14'N, *Earth Planet Sc Lett*, 225, 63–76, <https://doi.org/10.1016/j.epsl.2004.06.001>, 2004.
- 1281 Severmann, S., Johnson, C. M., Beard, B. L., and McManus, J.: The effect of early diagenesis
1282 on the Fe isotope compositions of porewaters and authigenic minerals in continental margin
1283 sediments, *Geochim Cosmochim Acta*, 70, 2006–2022,
1284 <https://doi.org/10.1016/j.gca.2006.01.007>, 2006.
- 1285 Sharma, M., Polizzotto, M., and Anbar, A. D.: Iron isotopes in hot springs along the Juan de
1286 Fuca Ridge, *Earth Planet Sc Lett*, 194, 39–51, [https://doi.org/10.1016/S0012-821X\(01\)00538-](https://doi.org/10.1016/S0012-821X(01)00538-6)
1287 6, 2001.
- 1288 Shelley, R. U., Roca-Martí, M., Castrillejo, M., Sanial, V., Masqué, P., Landing, W. M., van
1289 Beek, P., Planquette, H., and Sarthou, G.: Quantification of trace element atmospheric
1290 deposition fluxes to the Atlantic Ocean (>40°N; GEOVIDE, GEOTRACES GA01) during
1291 spring 2014, *Deep-Sea Res Pt I*, 119, 34–49, <https://doi.org/10.1016/j.dsr.2016.11.010>, 2017.
- 1292 Sieber, M., Conway, T. M., de Souza, G. F., Hassler, C. S., Ellwood, M. J., and Vance, D.:
1293 Isotopic fingerprinting of biogeochemical processes and iron sources in the iron-limited surface
1294 Southern Ocean, *Earth Planet Sc Lett*, 567, 116967, <https://doi.org/10.1016/j.epsl.2021.116967>,
1295 2021.
- 1296 Sieber, M., Lanning, N. T., Steffen, J. M., Bian, X., Yang, S.-C., Lee, J. M., Weiss, G., Hunt,
1297 H. R., Charette, M. A., Moore, W. S., Hautala, S. L., Hatta, M., Lam, P. J., John, S. G.,
1298 Fitzsimmons, J. N., and Conway, T. M.: Long Distance Transport of Subsurface Sediment-
1299 Derived Iron From Asian to Alaskan Margins in the North Pacific Ocean, *Geophys Res Lett*,
1300 51, e2024GL110836, <https://doi.org/10.1029/2024GL110836>, 2024.

- 1301 Slemons, L., Gorgues, T., Aumont, O., Menkes, C., and Murray, J. W.: Biogeochemical impact
1302 of a model western iron source in the Pacific Equatorial Undercurrent, *Deep Sea Research Part*
1303 *I: Oceanographic Research Papers*, 56, 2115–2128, <https://doi.org/10.1016/j.dsr.2009.08.005>,
1304 2009.
- 1305 Slemons, L., Murray, J. W., Resing, J., Paul, B., and Dutrieux, P.: Western Pacific coastal
1306 sources of iron, manganese, and aluminum to the Equatorial Undercurrent, *Global Biogeochem*
1307 *Cy*, 24, <https://doi.org/10.1029/2009GB003693>, 2010.
- 1308 Slemons, L., Paul, B., Resing, J., and Murray, J. W.: Particulate iron, aluminum, and manganese
1309 in the Pacific equatorial undercurrent and low latitude western boundary current sources, *Mar*
1310 *Chem*, 142–144, 54–67, <https://doi.org/10.1016/j.marchem.2012.08.003>, 2012.
- 1311 Sofen, L. E., Antipova, O. A., Buck, K. N., Caprara, S., Chacho, L., Johnson, R. J., Kim, G.,
1312 Morton, P., Ohnemus, D. C., Rauschenberg, S., Sedwick, P. N., Tagliabue, A., and Twining, B.
1313 S.: Authigenic Iron Is a Significant Component of Oceanic Labile Particulate Iron Inventories,
1314 *Global Biogeochemical Cycles*, 37, e2023GB007837, <https://doi.org/10.1029/2023GB007837>,
1315 2023.
- 1316 Sokolov, S. and Rintoul, S.: Circulation and water masses of the southwest Pacific: WOCE
1317 Section P11, Papua New Guinea to Tasmania, *J Mar Res*, 58, 2000.
- 1318 Stramma, L. and England, M. H.: On the water masses and mean circulation of the South
1319 Atlantic Ocean, *J Geophys Res-Oceans*, 104, 20863–20883,
1320 <https://doi.org/10.1029/1999JC900139>, 1999.
- 1321 Sutak, R., Camadro, J.-M., and Lesuisse, E.: Iron Uptake Mechanisms in Marine
1322 Phytoplankton, *Front. Microbiol.*, 11, <https://doi.org/10.3389/fmicb.2020.566691>, 2020.
- 1323 Swanner, E. D., Bayer, T., Wu, W., Hao, L., Obst, M., Sundman, A., Byrne, J. M., Michel, F.
1324 M., Kleinhanns, I. C., Kappler, A., and Schoenberg, R.: Iron Isotope Fractionation during Fe(II)
1325 Oxidation Mediated by the Oxygen-Producing Marine Cyanobacterium *Synechococcus* PCC
1326 7002, *Environ Sci Technol*, 51, 4897–4906, <https://doi.org/10.1021/acs.est.6b05833>, 2017.
- 1327 Tagliabue, A., Buck, K. N., Sofen, L. E., Twining, B. S., Aumont, O., Boyd, P. W., Caprara,
1328 S., Homoky, W. B., Johnson, R., König, D., Ohnemus, D. C., Sohst, B., and Sedwick, P.:
1329 Authigenic mineral phases as a driver of the upper-ocean iron cycle, *Nature*, 620, 104–109,
1330 <https://doi.org/10.1038/s41586-023-06210-5>, 2023.
- 1331 Talley, L. D.: Some aspects of ocean heat transport by the shallow, intermediate and deep
1332 overturning circulations, *Geoph Monog Series*, 112, 1–22,
1333 <https://doi.org/10.1029/GM112p0001>, 1999.
- 1334 Talley, L. D.: Freshwater transport estimates and the global overturning circulation: Shallow,
1335 deep and throughflow components, *Prog Oceanogr*, 78, 257–303,
1336 <https://doi.org/10.1016/j.pocean.2008.05.001>, 2008.
- 1337 Talley, L. D., Pickard, G. L., Emery, W. J., and Swift, J. H.: *Descriptive Physical*
1338 *Oceanography: An Introduction*, Academic Press, 555 pp., ISBN 978-0-7506-4552-2, 2011.
- 1339 Tian, H.-A., van Manen, M., Bunnell, Z. B., Jung, J., Lee, S. H., Kim, T.-W., Reichert, G.-J.,
1340 Conway, T. M., and Middag, R.: Biogeochemistry of iron in coastal Antarctica: isotopic
1341 insights for external sources and biological uptake in the Amundsen Sea polynyas, *Geochim*
1342 *Cosmochim Ac*, 363, 51–67, <https://doi.org/10.1016/j.gca.2023.10.029>, 2023.

- 1343 Tiangang, W., Kumul, C., Yuhao, Z., Mosusu, N., Bimin, Z., Pei, N., and De Vivo, B.: National-
1344 scale Geochemical Baseline of 69 elements in Papua New Guinea stream sediments, *J Geochem*
1345 *Explor*, 256, 107355, <https://doi.org/10.1016/j.gexplo.2023.107355>, 2024.
- 1346 [Tilliette, C., Taillandier, V., Bouruet-Aubertot, P., Grima, N., Maes, C., Montanes, M., Sarthou,](#)
1347 [G., Vorrath, M. E., Arnone, V., Bressac, M., González-Santana, D., Gazeau, F., and Guieu, C.:](#)
1348 [Dissolved Iron Patterns Impacted by Shallow Hydrothermal Sources Along a Transect Through](#)
1349 [the Tonga-Kermadec Arc, *Global Biogeochem Cy*, 36, e2022GB007363,](#)
1350 <https://doi.org/10.1029/2022GB007363>, 2022.
- 1351 Tomczak, M. and Godfrey, J. S.: *Regional Oceanography: An Introduction*, Daya Publishing
1352 House, 410 pp., ISBN 978-81-7035-306-5, 2003.
- 1353 Tomczak, M. and Hao, D.: Water masses in the thermocline of the coral sea, *Deep-Sea Res*, 36,
1354 1503–1514, [https://doi.org/10.1016/0198-0149\(89\)90054-X](https://doi.org/10.1016/0198-0149(89)90054-X), 1989.
- 1355 Tsuchiya, M.: The Origin of the Pacific Equatorial 13°C Water, *J Phys Oceanogr*, 11, 794–812,
1356 [https://doi.org/10.1175/1520-0485\(1981\)011<0794:TOOTPE>2.0.CO;2](https://doi.org/10.1175/1520-0485(1981)011<0794:TOOTPE>2.0.CO;2), 1981.
- 1357 Tsuchiya, M.: Flow path of the Antarctic Intermediate Water in the western equatorial South
1358 Pacific Ocean, *Deep-Sea Res*, 38, S273–S279, [https://doi.org/10.1016/S0198-0149\(12\)80013-](https://doi.org/10.1016/S0198-0149(12)80013-6)
1359 6, 1991.
- 1360 Tsuchiya, M. and Talley, L.: Water-property distributions along an eastern Pacific
1361 hydrographic section at 135W, *J Mar Res*, 54,
1362 https://elischolar.library.yale.edu/journal_of_marine_research/2191 (last access: 4 March
1363 2024), 1996.
- 1364 Tsuchiya, M., Lukas, R., Fine, R. A., Firing, E., and Lindstrom, E.: Source waters of the Pacific
1365 Equatorial Undercurrent, *Prog Oceanogr*, 23, 101–147, [https://doi.org/10.1016/0079-](https://doi.org/10.1016/0079-6611(89)90012-8)
1366 6611(89)90012-8, 1989.
- 1367 Waeles, M., Baker, A. R., Jickells, T., and Hoogewerff, J.: Global dust teleconnections: aerosol
1368 iron solubility and stable isotope composition, *Environ Chem*, 4, 233,
1369 <https://doi.org/10.1071/EN07013>, 2007.
- 1370 Wilson, E. L., Harpp, K. S., Schwartz, D. M., and Van Kirk, R.: The Geochemical Evolution
1371 of Santa Cruz Island, Galápagos Archipelago, *Front Earth Sci*, 10,
1372 <https://doi.org/10.3389/feart.2022.845544>, 2022.
- 1373 Winckler, G., Anderson, R. F., Jaccard, S. L., and Marcantonio, F.: Ocean dynamics, not dust,
1374 have controlled equatorial Pacific productivity over the past 500,000 years, *P Natl Acad Sci*
1375 *USA*, 113, 6119–6124, <https://doi.org/10.1073/pnas.1600616113>, 2016.
- 1376 Wyrski, K.: The Subsurface Water Masses in the Western South Pacific Ocean, *Mar Freshwater*
1377 *Res*, 13, 18–47, <https://doi.org/10.1071/mf9620018>, 1962.
- 1378 [Xiang, Y. and Lam, P. J.: Size-Fractionated Compositions of Marine Suspended Particles in the](#)
1379 [Western Arctic Ocean: Lateral and Vertical Sources, *Journal of Geophysical Research: Oceans*,](#)
1380 [125, e2020JC016144, <https://doi.org/10.1029/2020JC016144>, 2020.](#)
- 1381 Yeghicheyan, D., Bossy, C., Bouhnik Le Coz, M., Douchet, C., Granier, G., Heimbürger, A.,
1382 Lacan, F., Lanzanova, A., Rousseau, T. C. C., Seidel, J.-L., Tharaud, M., Candaudap, F.,
1383 Chmeleff, J., Cloquet, C., Delpoux, S., Labatut, M., Losno, R., Pradoux, C., Sivry, Y., and
1384 Sonke, J. E.: A Compilation of Silicon, Rare Earth Element and Twenty-One other Trace

- 1385 Element Concentrations in the Natural River Water Reference Material SLRS-5 (NRC-CNRC),
1386 Geostand Geoanal Res, 37, 449–467, <https://doi.org/10.1111/j.1751-908X.2013.00232.x>, 2013.
- 1387 Yeghicheyan, D., Aubert, D., Bouhnik-Le Coz, M., Chmeleff, J., Delpoux, S., Djouraev, I.,
1388 Granier, G., Lacan, F., Piro, J.-L., Rousseau, T., Cloquet, C., Marquet, A., Menniti, C., Pradoux,
1389 C., Freydier, R., Vieira da Silva-Filho, E., and Suchorski, K.: A New Interlaboratory
1390 Characterisation of Silicon, Rare Earth Elements and Twenty-Two Other Trace Element
1391 Concentrations in the Natural River Water Certified Reference Material SLRS-6 (NRC-
1392 CNRC), Geostand Geoanal Res, 43, 475–496, <https://doi.org/10.1111/ggr.12268>, 2019.
- 1393 Yuan, X. and Talley, L. D.: Shallow Salinity Minima in the North Pacific, J Phys Oceanogr,
1394 22, 1302–1316, [https://doi.org/10.1175/1520-0485\(1992\)022<1302:SSMITN>2.0.CO;2](https://doi.org/10.1175/1520-0485(1992)022<1302:SSMITN>2.0.CO;2), 1992.
- 1395 Zheng, L. and Sohrin, Y.: Major lithogenic contributions to the distribution and budget of iron
1396 in the North Pacific Ocean, Sci Rep, 9, 11652, <https://doi.org/10.1038/s41598-019-48035-1>,
1397 2019.